Localized steady and oscillatory states near a Turing-Hopf instability in a semiconductor model

Fahad Al Saadi*, Edgar Knobloch♯, Alexander Meiners♢, Hannes Uecker★

* Department of Systems Engineering, Military Technological College, Muscat, Oman, fahad.alsaadi@mtc.edu.om,
♯ Department of Physics, University of California, Berkeley, CA 94720, USA, knobloch@berkeley.edu,
♢,★ Institut für Mathematik, Universität Oldenburg, D26111 Oldenburg, alexander.meiners@uni-oldenburg.de, hannes.uecker@uni-oldenburg.de

August 19, 2024

Abstract

Numerical continuation is used to study the interaction between a finite wave number Turing instability and a zero wave number Hopf instability in a two-species model of a semiconductor device. The model admits two such codimension-two interactions, both with a subcritical Turing branch that is responsible for the presence of spatially localized Turing states. The Hopf branch may also be subcritical. We uncover a large variety of spatially extended and spatially localized states in the vicinity of these points and by varying a third parameter show how disconnected branches of time-periodic spatially localized states can be "zipped up" into snaking branches of time-periodic oscillations. These are of two types: a Turing state embedded in an oscillating background, and a breathing Turing state embedded in a non-oscillating background. Stable two-frequency states resembling a mixture of these two states are also identified. Our results are complemented by direct numerical simulations. The findings explain the origin of the large multiplicity of localized steady and oscillatory patterns arising from the Turing-Hopf interaction and shed light on the competition between them.

Contents

1 Introduction

The interaction of Hopf and Turing instabilities in two-component reaction-diffusion (RD) systems may yield a multitude of stable spatiotemporal patterns, both spatially extended and spatially localized. These include time-dependent domain-filling Turing-Hopf mixed modes (THMM, see Table 1 for a list of acronyms) consisting of inclusions of a Turing state within an oscillating background or vice versa, separated by more-or-less stationary fronts, as well as localized breathing states (LSW) embedded in a stationary homogeneous background. These states differ in their origin. The former are present in regions of bistability between extended Turing and Hopf states, while the latter are associated with subcritical bifurcations, for example, a subcritical Turing state that coexists with a supercritical Hopf state or a subcritical Hopf state that coexists with a stable homogeneous state. The properties of these states are determined by the order of the primary Turing and Hopf bifurcations and the criticality of the resulting branches, and are best studied in the vicinity of codimension-2 points where the two instabilities occur simultaneously. This approach was first used in a study of the Turing-Hopf interaction in the Brusselator RD model [DWLDB96], with follow-up studies in [TMV09, TBMV11, TMB$^+$13].

Subsequent work on the dynamics of patterns near a codimension-2 Turing-Hopf (C2TH) point employed a two-component RD model for semiconductor devices [MDWBS97] hereafter referred to as the SECO model. This model exhibits two C2TH points in the parameter space of the model, and numerical time integration, hereafter direct numerical simulation (DNS), revealed different spatiotemporal behavior in their vicinity. The SECO model is important not only for its experimental realizability but also because it exhibits a larger variety of structures than other RD models owing to the possibility of subcritical Turing or Hopf branches as parameters vary [Uec21a]. The goal of the present work is to elucidate the properties of these structures using numerical continuation to trace the origin of these structures rather than relying solely on DNS and to use this model to describe behavior that we believe to be generic in two-species RD systems, rather than focusing on the physical consequences on the states we identify.

The above work shows that THMM patterns may come in branches that snake back and forth across parameter space adding one spatial period to the Turing pattern after every two folds, behavior that is very similar to the well-known snaking of stationary localized Turing patterns over a (spatially and temporarily) constant background, hereafter localized steady states (LSS), that are present in numerous pattern-forming systems. This behavior is associated with approach to a homoclinic or heteroclinic cycle in space, and is somewhat loosely referred to as homoclinic snaking, see, e.g., [Pom86, WC99, CK09, BK07, Kno08, BKL$^+$09, UW14, KUY21] and the references therein for background and examples. In addition to such snaking THMM branches we show here that THMM states may also come as "long or short connections" both bifurcating from and reconnecting to the LSS branch, as well as in the form of a stack of isolas, i.e. branches that are disconnected from all others.

In [AKNU24] we described a mechanism whereby these two sorts of THMM branches may be related to one other employing two-parameter continuation in a two-component predator-prey model [Zho19] and a two-component vegetation-water model [vHPPRM04], see also [APR23]. In particular, we demonstrated, for instance by varying the diffusivity ratio D as a second parameter, that we can "zip up" certain stacks of short THMM branches into much longer THMM branches exhibiting snaking. In a nutshell, this happens because the secondary Hopf points (HPs) responsible for the bifurcations/reconnections of the THMM connections to the LSS snake can only annihilate *in fold points of the LSS snake* as D varies. These annihilation events connect up adjacent THMM segments and occur in rapid succession. At other locations on the LSS branch the Hopf points generically pass through one other and no zipping up takes place.

We reconsider the SECO model from [MDWBS97, Uec21a],

$$\begin{aligned} \partial_t u_1 &= \partial_x^2 u_1 + \frac{u_2 - u_1}{(u_2 - u_1)^2 + 1} - \tau u_1, \\ \partial_t u_2 &= D\partial_x^2 u_2 + \alpha[j_0 - (u_2 - u_1)], \end{aligned} \tag{1}$$

which we consider on an interval $\Omega = (-l, l)$, $l > 0$ and sufficiently large, with homogeneous Neumann boundary conditions (BCs), $\partial_x u_1 = \partial_x u_2 = 0$ on $\partial\Omega$. The model describes charge transport in a layered semiconductor; u_1 is the interface charge in the device, u_2 is a normalized voltage across it, and $(j_0, \alpha, D, \tau) \in \mathbb{R}^4$ is a parameter vector. The unique spatially homogeneous steady state is

$$u^* = (u_1^*, u_2^*), \quad u_1^* = \frac{j_0}{\tau(j_0^2 + 1)}, \quad u_2^* = j_0 + u_1^*. \tag{2}$$

For the linear stability analysis of this state (see §2) we initially fix $(D, \tau) = (6.5, 0.05)$, and discuss the stability of u^* in the (j_0, α) parameter plane. This analysis yields two curves, $\alpha = \alpha_T(j_0)$ and $\alpha = \alpha_H(j_0)$, of (primary) Turing (resp. Hopf) bifurcations.

The two curves intersect at two codimension-2 Turing-Hopf points (C2TH points), hereafter referred to as $\mathrm{C2TH}_{1,2}$. Near $\mathrm{C2TH}_1$ u^* loses stability to a supercritical Hopf bifurcation followed by a subcritical Turing bifurcation and we observe a zipping up of THMM segments when D varies. Moreover, in this regime the model also exhibits localized breathing states referred to as standing waves (LSW), and these, like the THMM segments, can be zipped up into a snaking branch, or unzipped into a stack of disconnected LSW segments. On the other hand, near $\mathrm{C2TH}_2$ we can start with a similar "stack of THMM connections" between HPs on an LSS snake, with collisions of HPs at the folds of the LSS snake as D varies, but this time on the "wrong side", and this has a very different effect: Instead of zipping/unzipping, when D is increased the (long) THMM connections detach as isolas, while for decreasing D the branches split into short connections that remain attached to the LSS and disconnected isolas. The short connections then vanish together with their HPs when these collide upon further decrease of D. Thus, instead of the THMM connections zipping up into a snake, we end up with a stack of THMM isolas. Moreover, these isolas may themselves shrink to zero with further change in D and disappear.

Table 1: Acronyms

BD	bifurcation diagram	BP/FP/HP	branch/fold/Hopf point
FPC	fold point continuation	HPC	Hopf point continuation
LSS	localized steady state	(L)SW	(localized) standing wave
PO	(time) periodic orbit	POC	periodic orbit continuation
C2TH	codimension-2 Turing-Hopf (point)	DNS	direct numerical simulation
MM	mixed mode	THMM	Turing-Hopf mixed mode

For mixed modes we also employ notation such as **TH2MM** for a Turing—Hopf2–mixed mode, where Hopf2 means the sideband Hopf mode with a spatial period comparable to the domain size, and **LSW-H-MM** for a LSW-Hopf-mixed mode, i.e., a localized SW on the left of the domain and a (spatially uniform) PO on the right, or **H-LSW-H-MM** for a PO on the left, a LSW in the middle, and again a PO on the right; occasionally we augment this as, e.g.,
2T-H-MM for a Turing mode with two peaks on the left and a (uniform) PO on the right, or
2LSW-H-MM for a 2-peak LSW on the left and a (uniform) PO on the right.

Plan of the paper. In §2 we fix the parameter (ranges) for the SECO model and review the linear stability of its unique homogeneous steady state u^*, thereby introducing the two C2TH points $\mathrm{C2TH}_{1,2}$. Section 3 is devoted to the use of numerical continuation and bifurcation theory to study

the nonlinear behavior near both these points. In §3.1 we focus on the vicinity of $\mathrm{C2TH}_1$, finding a multitude of short THMM segments bifurcating from LSS, and an LSW snake. We then show how by varying D we can zip up the THMM segments into a THMM snake, while at the same time the LSW snake unzips into LSW segments. We can use the time scale τ in a similar way to zip/unzip solution branches, but not α. In §3.2 we discuss the very different behavior near $\mathrm{C2TH}_2$. Near both $\mathrm{C2TH}_1$ and $\mathrm{C2TH}_2$ we also run some direct numerical simulations (DNS) to illustrate the stability/instability of a number of states found by continuation and branch switching, and identify some further (classes of) spatio-temporal states. In §4 we conclude with a short summary and discussion.

Owing to the high multiplicity, diversity and competition between various patterns and localized steady and time-periodic states in this system, we have to make a rather severe selection of the branches shown in the bifurcation diagrams (BDs). Nevertheless, some of the BDs are rather complicated and best explored interactively, and for this we recommend the software download at [Uec24], and the movies (see Appendix A) that go through the BDs step by step.

2 Stability and instability of the homogeneous steady state

Denoting the terms without derivatives in (1) by f, the linearization of (1) at $u^* = (u_1^*, u_2^*)$ has the form

$$\partial_t v = L(\partial_x)v := D\partial_x^2 v + \partial_u f(u^*)v \tag{3}$$

with a constant-coefficient differential operator $L(\partial_x)$, where $\mathcal{D}$ =diag$(1, D)$. For $x \in \mathbb{R}$, (3) has solutions of the form

$$v(t, x) = \mathrm{e}^{\mu(k)t + \mathrm{i}kx}\phi(k), \tag{4}$$

where $k \in \mathbb{R}$ is called the wave number, $\mathrm{e}^{\mathrm{i}kx}\phi(k)$ is called a (Fourier-)mode, and $(\mu(k), \phi(k)) \in \mathbb{C}\times\mathbb{C}^2$ is an eigenpair of $\hat{L}(\mathrm{i}k) := -k^2\mathcal{D} + \partial_u f(u^*) \in \mathbb{R}^{2\times 2}$. The functions

$$k \mapsto \mu_{1,2}(k), \tag{5}$$

give the dispersion relation, where for each k we sort the eigenvalues such that $\mathrm{Re}\mu_2(k) \le \mathrm{Re}\mu_1(k)$, so that the dispersion relation is approximated by $k \mapsto \mu_1(k)$. Over $\Omega = (-l, l)$ we additionally have to fulfill the assumed Neumann BCs, which restricts k to the (dual) lattice $\mathcal{L} = \pi\mathbb{Z}/(2l)$. The solution u^* is stable if $\mathrm{Re}\mu_1(k) < 0$ for all $k \in \mathcal{L}$, unstable if there exists a k such that $\mathrm{Re}\mu_1(k) > 0$, and instabilities and bifurcations may occur if there is a $k = k_c$ such that $\mathrm{Re}\mu_1(k_c) = 0$. The instability is called a *long wave instability* if $k_c = 0$ and $\mathrm{Im}\mu_1(k_c) = \mathrm{Im}\mu_2(k_c) = 0$; it is a *Hopf instability* if $k_c = 0$ and $\mathrm{Im}\mu_1(k_c) = \mathrm{Im}\mu_2(k_c) \neq 0$, while for $k_c \neq 0$ (and consequently $\mathrm{Im}\mu_1(k_c) = 0$) it is called a *Turing instability*. We note that solutions satisfying Neumann BCs can be reflected in the boundaries at $x = \pm l$ thereby generating solutions satisfying periodic boundary conditions on a domain of length $4l$. [1]

Figure 1(a) shows the Turing (blue) and Hopf (red) marginal stability curves in the (j_0, α) plane. These curves can be computed analytically, see [MDWBS97] (for $\Omega = \mathbb{R}$), but here we compute them numerically by branch point (BP) continuation and Hopf point (HP) continuation (see [Uec21b, §3.5]) on $\Omega = (-l, l)$, $l = 200$, chosen large enough to get a good sampling of the dispersion relation. Sample dispersion relations are shown in panels (b)-(d) where the $*$s indicating the allowed values of k over Ω. For given j_0, the steady state u^* is stable for α above the maximum of the red and blue

[1] A primary instability with $k_c \neq 0$ and $\mathrm{Im}\mu_1(k_c) = -\mathrm{Im}\mu_2(k_c) \neq 0$ is called a *wave instability*, but in RD systems this requires at least three components.

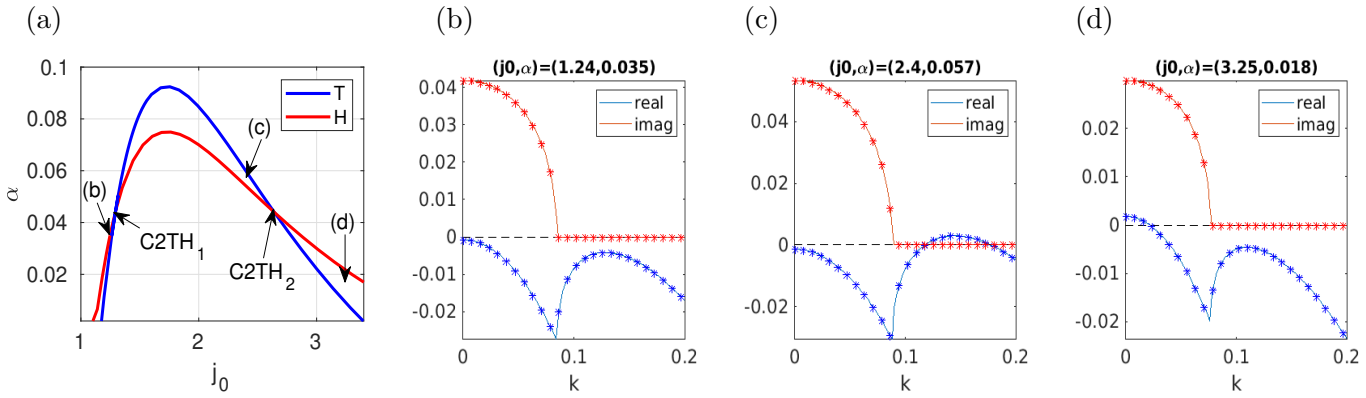

Figure 1: (a) Turing and Hopf bifurcation lines in the (j_0, α) plane as obtained from BP and HP continuation. Sample dispersion relations $\mu_1(k)$ for (b) a linearly stable case near $\mathrm{C2TH}_1$, (c) a Turing-unstable case, and (d) a Hopf-unstable case, with (j_0, α) as indicated. The remaining parameters are (D, τ)=(6.5, 0.05). The $*$s in (b)-(d) show the allowed wave numbers on the interval Ω=$(-l, l)$ with l=200 and Neumann BCs.

lines. As we decrease α at fixed j_0 (or increase j_0 from 1.1 or decrease it from 3 at fixed $\alpha = 0.05$, say) we either first cross the blue line, meaning that u^* loses stability to a Turing mode, or the red line, meaning that u^* loses stability to a Hopf mode. There are two codimension-2 Turing-Hopf points, $\mathrm{C2TH}_1$ at $(j_0, \alpha)^* \approx (1.295, 0.0441)$ and $\mathrm{C2TH}_2$ at $(j_0, \alpha)^\star \approx (2.65, 0.0438)$. In any neighborhood of these, the first instability can be either to a Hopf or to a Turing mode. As one enters deeper into the instability region the interval of unstable wave numbers grows, resulting in the destabilization of sidebands of the primary Turing ($k_c \neq 0$) or Hopf ($k_c = 0$) modes in quick succession.

In [Uec21a] we considered Turing and Hopf bifurcations from u^* near the *right* C2TH point $\mathrm{C2TH}_2$ (resp. its analog for $D = 8$), both of which were found to be subcritical, with the Turing branch responsible for the presence of snaking branches of LSS patterns. From the latter bifurcate some segments of THMM, with rather weak (small amplitude) oscillations of the background, before they return to the LSS branch from which they bifurcate. Additionally, we constructed a TH-front by splicing together a T mode and an H mode at some initial (j_0, α). This yields a branch with larger amplitude oscillations of the homogeneous background, but we were unable to determine where this branch bifurcates from or connects to. In the present work we select the numerically more convenient parameter value $D = 6.5$ and are able to elucidate much additional detail concerning the transitions in the neighborhood of $\mathrm{C2TH}_2$.

In §3.1 we start, however, with a detailed study of the neighborhood of the *left* C2TH point $\mathrm{C2TH}_1$, where the basic behavior of the T, H and LSS branches is similar to that near $\mathrm{C2TH}_2$ but the behavior of the THMM branches is quite different, but somewhat simpler than that near $\mathrm{C2TH}_2$ in the sense that we can use the LSS snakes as skeletons not only for the steady states but also for THMM and LSW. As a result we are able to classify comprehensively the bifurcations from the LSS snakes in terms of THMM and LSW, and use this fact to manipulate the bifurcations leading to them to zip them up or unzip them. The situation near $\mathrm{C2TH}_2$ turns out to be somewhat more complicated and is therefore postponed to §3.2.

3 Numerical continuation and bifurcation

For basics of numerical continuation and bifurcation, and the basic ideas of the package `pde2path`, we refer to [Uec21b, Uec21a]. We first look for bifurcations of steady state branches and time-periodic orbit (PO) branches from the trivial (spatially homogeneous, steady) branch $j_0 \mapsto u^*$ with the other parameters (α, D, τ) initially fixed. These bifurcations yield Turing branches (steady,

spatially periodic solutions) or Hopf branches (time-periodic, spatially homogeneous solutions, or somewhat more generally spatially periodic with a large wavelength, i.e. with sideband wave numbers $0 < k \ll 1$). Subsequently, we can look for secondary bifurcations from the Turing and Hopf branches, and thus obtain bifurcation diagrams (BDs). Due to the large variety of bifurcations and associated patterns we find, these BDs are necessarily "partial", i.e., we are forced to focus on some (classes of) branches only. In such a study, stability is an important issue, and for the steady state branches we indicate stable parts (according to linearized stability, i.e., the eigenvalues of the linearized operator) by thicker lines. For POs, the stability is computed from the Floquet spectrum, which is generally expensive, see, e.g., [Uec21b, §3.4.2], and we do not in general compute the Floquet multipliers along with the branches (but see, e.g., Fig.5). Instead, we compute the Floquet multipliers *a posteriori* and comment on the resulting stability properties of the POs in the text.

Even with a severe selection of "important" branches, the partial BDs quickly become rather complex, and we refer to the Appendix for movies going through the BDs step by step, and showing the Floquet multipliers of the POs. Moreover, we identify further classes of solutions of (1) by direct numerical simulation (DNS). These consist of a mix of LSW and (background) Hopf oscillations, LSW-H-MM for short, and are in general quasiperiodic in time (except in the case of resonance).

As in [Uec21a] (and also [AKNU24]), to plot BDs for (1), we use the "norm" $\|u\|_2$ defined as

$$\text{(a)}\quad \|u\|_2^2 = \frac{1}{|\Omega|}\int (u_1(x)-u_1^*)^2\,\mathrm{d}x, \qquad \text{or}\quad \text{(b)}\quad \|u\|_2^2 = \frac{1}{T|\Omega|}\int_0^T\int (u_1(t,x)-u_1^*)^2\,\mathrm{d}x\,\mathrm{d}t, \tag{6}$$

for steady states and POs, respectively, such that $\|u\|_2 = 0$ means $u_1 \equiv u_1^*$. This gives a better graphical separation of the branches in the BDs than using a proper norm such as $\|u\|_{L^2}^2 = \frac{1}{|\Omega|}\int u_1^2 + u_2^2\,\mathrm{d}x$.

3.1 Vicinity of C2TH$_1$

3.1.1 Basic branches at $D = 6.5$

Figure 2, with further details in Fig. 3, shows a "basic" (see Remark 3.1 for what we mean by that) bifurcation diagram in j_0 with $(\alpha, D, \tau) = (0.035, 6.5, 0.05)$ fixed. The figure shows *two* types of steady state branches, and *three* types of PO branches. We start the discussion with two Turing branches (blue) that bifurcate from $u \equiv u^*$. The first, T1 (light blue, 8 waves, profile A) bifurcates subcritically but never reaches the j_0 values where u^* is stable. In contrast, T22 (dark blue, 6 waves, profile B) reaches farthest to the left of all the Turing branches bifurcating from u^* up to $j_0 = 1.3$, resulting in a short stable segment after its fold near $j_0 = 1.238$. The intervening Turing branches are omitted. Since T1 is subcritical we expect a branch of LSS to bifurcate from it. This branch (orange) bifurcates from the first BP on T1 and corresponds to the "standard" snaking branch of LSSs [BK07], sample solution profiles at locations HP3 and HP40, i.e, at the third and 40th Hopf points along the orange branch.[2] As usual, after every two folds along the LSS branch the solution adds one pattern wavelength. The branch exhibits a short stable segment after its first fold on the left, leading to bistability between the corresponding LSS and the stable trivial state u^*; when the growing LSS fill the domain the branch terminates on T22 near its fold. This termination point is an Eckhaus bifurcation.

The primary Hopf branches H1 and H3 are shown in shades of brown and bifurcate supercritically from u^*. Of these H1 is a pure $k = 0$ Hopf mode and is stable throughout, sample profile C (C′

[2]We call LSS a branch of localized steady states even though solutions on it resemble a front connecting a Turing pattern to u^*. However, as already mentioned the use of Neumann BCs allows us to reflect these solutions in $x = -l$ to generate a genuine LSS.

shows the same solution in a 3D plot).[3] In contrast, H3 starts out as a sideband Hopf branch (with $k = \pi/200$) but after a fold it reconnects to T1, and hence is classified here as a THMM, see sample profile B. This solution is unstable throughout. To avoid clutter we omit H2 (with $k = \pi/400$), which behaves similarly. A further branch T1-H3 (grey) bifurcates from T1 and reconnects to it. Solutions on this branch take the form of breathing oscillations of the Turing pattern. We refer to this state as a *standing wave* (SW), see sample profile E. Note that genuine SWs (with $O(1)$ wave vector k, as opposed to the Hopf sidebands $0 < k \ll 1$) cannot bifurcate directly from a homogeneous state in our two-component RD system, cf. Footnote 1.

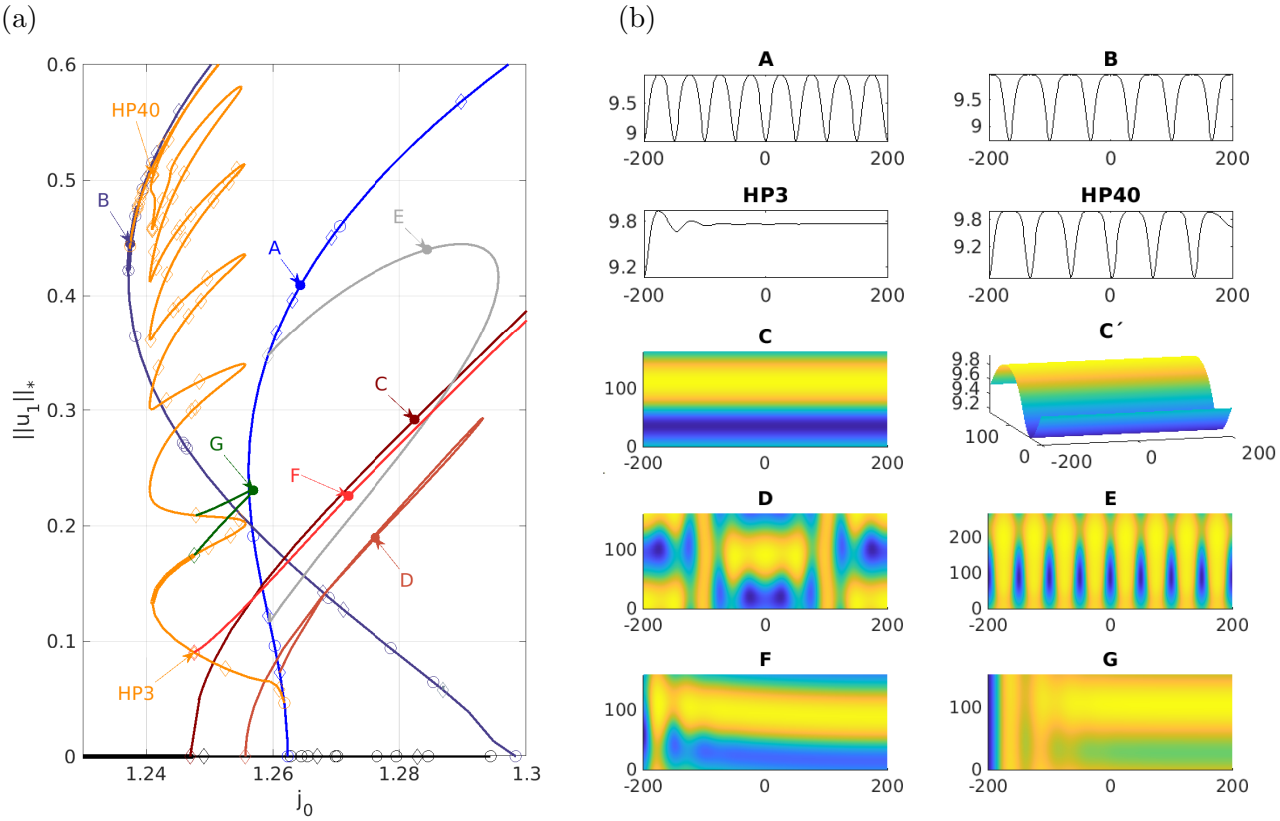

Figure 2: (a) Partial BD near C2TH$_1$ with $(\alpha, D, \tau) = (0.035, 6.5, 0.05)$, showing two Turing branches T1 (blue) and T22 (dark blue) that bifurcate from u^*, and the LSS branch T1-1 (orange) that bifurcates from T1 and reconnects to T22. Hopf branches H1 (dark brown) and H3 (lighter brown) also bifurcate from u^* (with H3 reconnecting to T1), while the Hopf branch T1-H3 bifurcates (grey) from T1 and then reconnects to it; the THMM branch bifurcates from T1-1/HP3 (red) and extends to large j_0. The figure also shows a THMM segment (green) bifurcating from T1-1/HP4 and reconnecting to T1-1/HP8.

We next turn to the various HPs on the LSS branch. These give rise to oscillating states of four different types. First, there is the red THMM branch bifurcating from LSS/HP3, with uniform oscillations of the background to the right of the localized Turing state, see sample profile F; this branch extends to large j_0 with a gradual increase in the amplitude of the background oscillations. However, this background oscillation is not strictly homogeneous, and exhibits a weak spatial phase gradient (small wave number). As a result this state can also be interpreted as a traveling wave (TW) running into the localized state near $x = -200$. We return to this observation in Figs. 6 and 8. Then there is the green branch that bifurcates from HP4 on LSS and reconnects to it at HP8. As shown in

[3] In what follows we mostly restrict to top view plots and, to avoid clutter, omit colorbars. We always have minima in blue and maxima in yellow, and all solutions vary roughly between $\min u_1 \approx 9$ and $\max u_1 \approx 10$. Moreover, u_2 varies within a similar range and is generally in phase with u_1, and thus for simplicity we plot u_1 only. However, the movies show plots of both u_1 and u_2.

sample profile G, this branch consists of POs with a narrow Turing pattern on the left while a large part of the domain oscillates homogeneously, albeit with a rather small amplitude (compare profile G with C or F) and no background phase gradient. There are in fact many such branch segments encountered repeatedly as one proceeds up the LSS branch.

We show the third type of solution generated in HPs on the LSS branch in Fig. 3. There is a very short lighter green TH2MM segment connecting HP6 and HP7 (sample profile E), corresponding to an interaction of LSS and the solutions on H2 with a nonzero background wave number. As the Turing parts of the solutions along LSS expand and the homogeneous parts shrink further up the LSS snake, there are further THMM connections, for instance connecting HP14 and HP15 (sample profile H), and altogether 40 HPs before the LSS snake reconnects to T22, the Turing branch with $k = 3\pi/200$ bifurcating from the 22nd BP on the trivial branch.

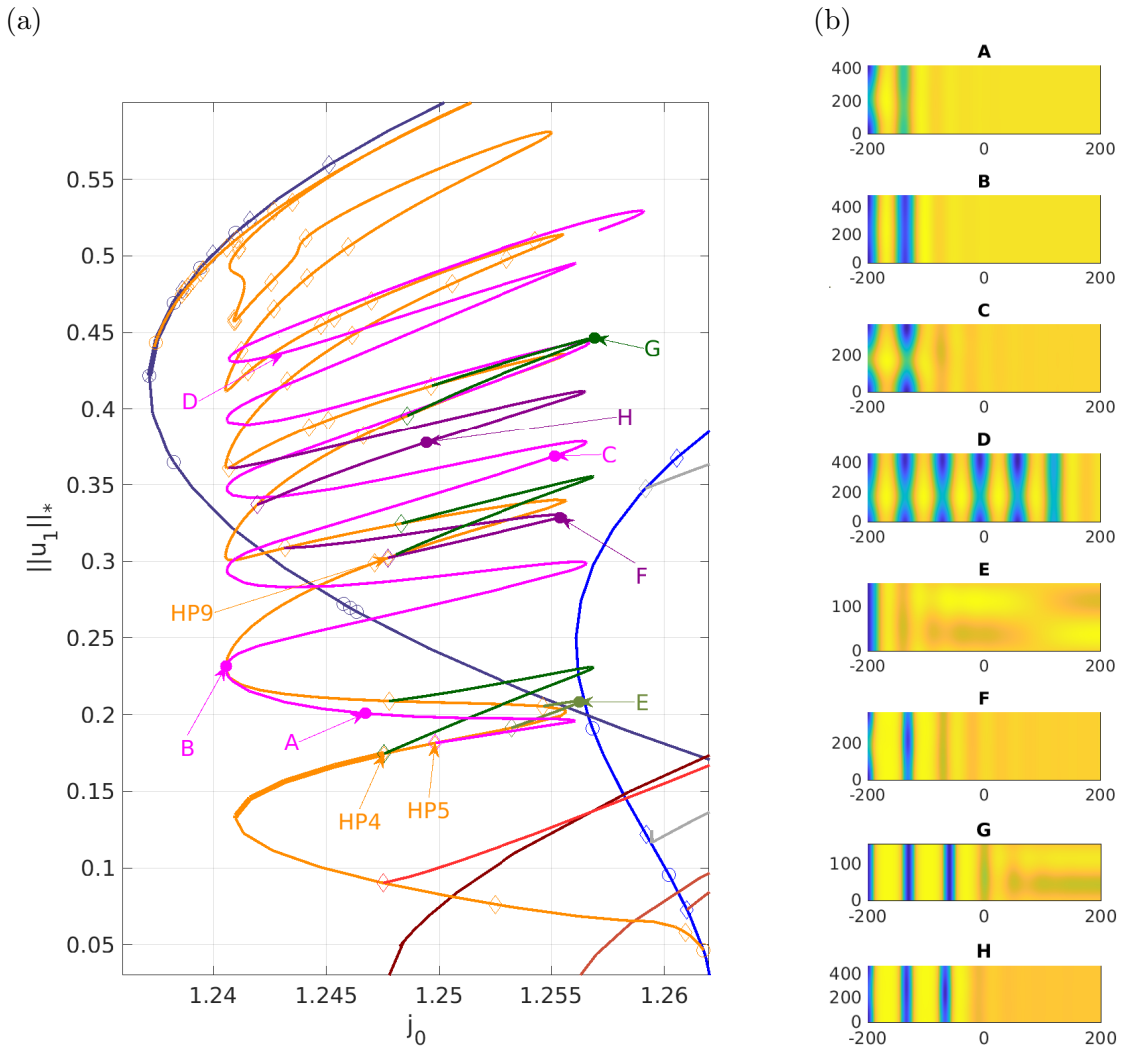

Figure 3: Figure 2 continued, showing three THMM segments (dark green) and a TH2MM segment (lighter green) bifurcating from the LSS branch T1-1 (orange). A snaking branch of LSW (magenta) bifurcating from T1-1/HP5 is also shown, as are disconnected LSW segments (violet). Past the top fold on the magenta branch the different trough oscillations go out of synchrony and the solution ceases to be periodic in time and can no longer be followed.

At this stage we may suspect (guided by the experience from, e.g., [AKNU24]) that the stacking of the green branches is one possibility for the organization of THMM states, while the other are long snaking branches of THMM states, with the addition of further Turing wavelengths to the THMM no longer mediated by the LSS snake, but directly occurring in a THMM snake. We call the process of turning a stack of THMM segments into a snake "zipping up", and show below how that can be

achieved by continuation in D (as in [AKNU24]).

In contrast to the systems (and parameter regimes) considered in [AKNU24], we find here a fourth type of POs that bifurcate from the orange snake, namely localized standing waves (LSW). In particular, there is a snaking branch of *in-phase* LSW (magenta, sample profiles A-D). This branch bifurcates from HP5 on LSS, and adds one spatial wavelength to the breathing peaks (or here troughs) after every pair folds. Some parts of the branch (near the left folds) contain stable solutions (see movies). Additionally, higher up the LSS snake there are HPs where localized *out-of-phase* oscillating troughs appear, see samples profiles F and G, but like the THMM states these form short segments connecting LSS to LSS instead of a longer snake. Localized SW snakes and isolas are also computed in [ACV24]. From this work, and from the intuition gained in zipping up THMM, we may suspect that the "long" LSW snake is only one possibility of how LSW, or bifurcations of LSW from LSS, can be organized, the other possibility being stacks of short segments, as for the THMM branches or the LSW branches (magenta, profiles F and H). Indeed, we find below that the magenta snake is (partly) "unzipped" when the green stacks zip up.

Note that HP4 and HP6 for bifurcation of THMM and HP5 for the LSW are close together, and hence have very similar profiles. However, the frequencies ω (temporal period $2\pi/\omega$) and the associated eigenfunctions are very different (see Fig. 5). In fact, this is the reason why the different HPs (for THMM vs LSW) just "pass through each other" when varying a second parameter, while similar HPs (e.g. two THMM HPs, or two LSW HPs) "collide", which may yield annihilation. In Fig. 4 we show the period T along selected branches from Fig. 2 and Fig. 3. For the (green) THMM branches the period is set in a narrow range $T \in (151, 155)$ by the background oscillation H1, while for the (light green) TH2MM branch it follows that of H2. The periods for the LSW branches in (b) vary more strongly, $T \in (350, 490)$, and are always at least 2.25 times that of the THMM branches.

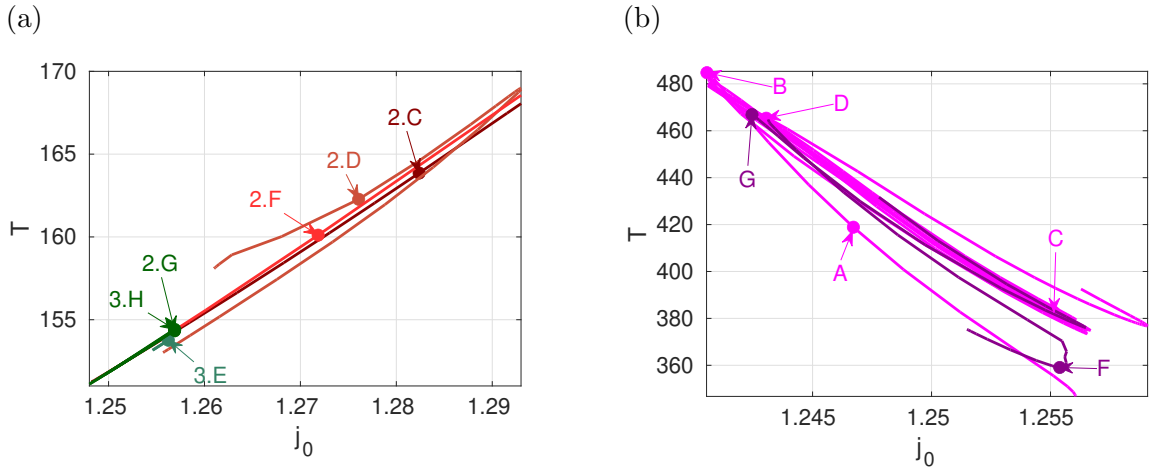

Figure 4: Period T along PO branches from Figs. 2 and 3 (same color code). In (a), the notation 2.* refers to profiles from Fig. 2, and 3.* to profiles from Fig. 3. In (b) all letters refer to profiles from Fig. 3.

Remark 3.1 While the partial BD in Figs. 2 and 3 is already quite complex, to avoid clutter it leaves out a number of further interesting branches. First, there are many further BPs and HPs on the trivial branch $u \equiv u^*$. We focus on just two Turing branches and two Hopf branches: H1 is key since this is where u^* loses stability. It yields a branch of homogeneous oscillations, stable throughout the displayed range, but these homogeneous oscillations are not of our primary interest. H3 is interesting despite being unstable because it folds back and reconnects to T1. A similar behavior is seen for H2, which is therefore omitted.

We show T1 (and the subsequent LSS=T1-1 branch) because it is the first Turing branch that bifurcates from $u = u^*$. However, it is *not* more relevant or interesting than later Turing branches,

such as T22, which extends farthest to the left and is the termination of the LSS branch. Moreover, this branch, unlike T1, contains a short stable part (after its fold).[4] On all of these Turing branches there are further BPs and HPs, which lead to similar behavior as that on T1. Namely, the HPs on the Turing branches yield SWs (without spatial localization), such as T1-H3, sample G in Fig. 2. The first steady BP on each of these Turing branches leads to LSSs like the orange branch, while BPs higher up on the Turing branches yield snaking branches of "multi–bump" LSSs (not shown). On many of these LSSs we then again find BPs and HPs like on the orange branch, leading to THMM and to LSW.

Thus the branches and corresponding solutions come in various different versions, with different spatial and temporal wavelengths, for example, as shown in Fig. 2(a), and the idea of Figs. 2 and 3 is to provide a selection of illustrative branches and the corresponding solutions. ⌋

3.1.2 Intermezzo 1: PO stability and bifurcations

In the BD plots we generally do *not* indicate stability/instability of the PO branches; this is partly because for reasons of speed we do not compute the multipliers as part of the continuation process, but more importantly because the BDs are already somewhat cluttered. Instead we refer to the movies (Appendix A) which go step by step through the BDs, and plot the (steady or PO) solutions together with linearization spectra, resp. Floquet multipliers. We remark that only a small number of the POs are in fact stable. In particular, of the green THMM branches in Fig.3, only the initial part of the first THMM branch is stable, see Fig. 5 and Fig. 2, profile G. This is expected since HP4 is a supercritical bifurcation and takes place on a stable LSS branch (thick orange line). Following the green branch from HP4 one finds that it soon loses stability via a torus (or Neimark–Sacker) bifurcation. In contrast to "easy" PO bifurcations (multiplier going through 1) and PO period-doubling bifurcations (multiplier going through -1), we currently cannot handle these directly in `pde2path`. However, the DNSs in Fig. 5(b,c) indicate that this bifurcation is also supercritical, with stability transferred to the resulting two-frequency state. The new frequency manifests itself in oscillations near the left domain boundary with negligible effect at the right boundary, and the amplitude of these oscillations increases as one follows the resulting torus branch to larger j_0. The resulting two-frequency state therefore consists of a breathing Turing part near the left boundary, which we consider as "inherited" from the LSW bifurcation from LSS at HP5, embedded in a $k = 0$ background state that oscillates with a different frequency.

Like the torus bifurcation shown in Fig. 5(g), we find PO bifurcations, of pitchfork, period-doubling and torus type on all of the THMM and LSW branches that bifurcate from the LSS branch. Figure 5(a) shows a detail of the magenta LSW branch from Fig. 3 with stability information, showing that the LSW states are only stable on a short segment after the first left fold. We again refer to the movies in Appendix A, and to §3.1.3 for "typical" dynamical behavior.

3.1.3 Intermezzo 2: DNS

In Figures 2 and 3 we found two classes of POs bifurcating from the (orange) LSS snake, namely localized breathing or standing waves (LSW, magenta and violet branches), and Turing-Hopf-Mixed Modes (THMM, green branches). The LSW can be *in phase* (profiles 3.A-D), or have various phase shifts between adjacent peaks/troughs, e.g., 3.F and 3.G, all the while remaining periodic in time. However, at the top of the snake there are further HPs (HP16-HP40), for which we do not present the bifurcating branches. These are of various types, mostly of LSW type, but sometimes with defect-like structure in which one of the troughs oscillates with a markedly smaller amplitude. All appear to be

[4] See also [AKNU24, III.B] for discussion of strong subcriticality of non-primary Turing branches, and its implications for localized patterns.

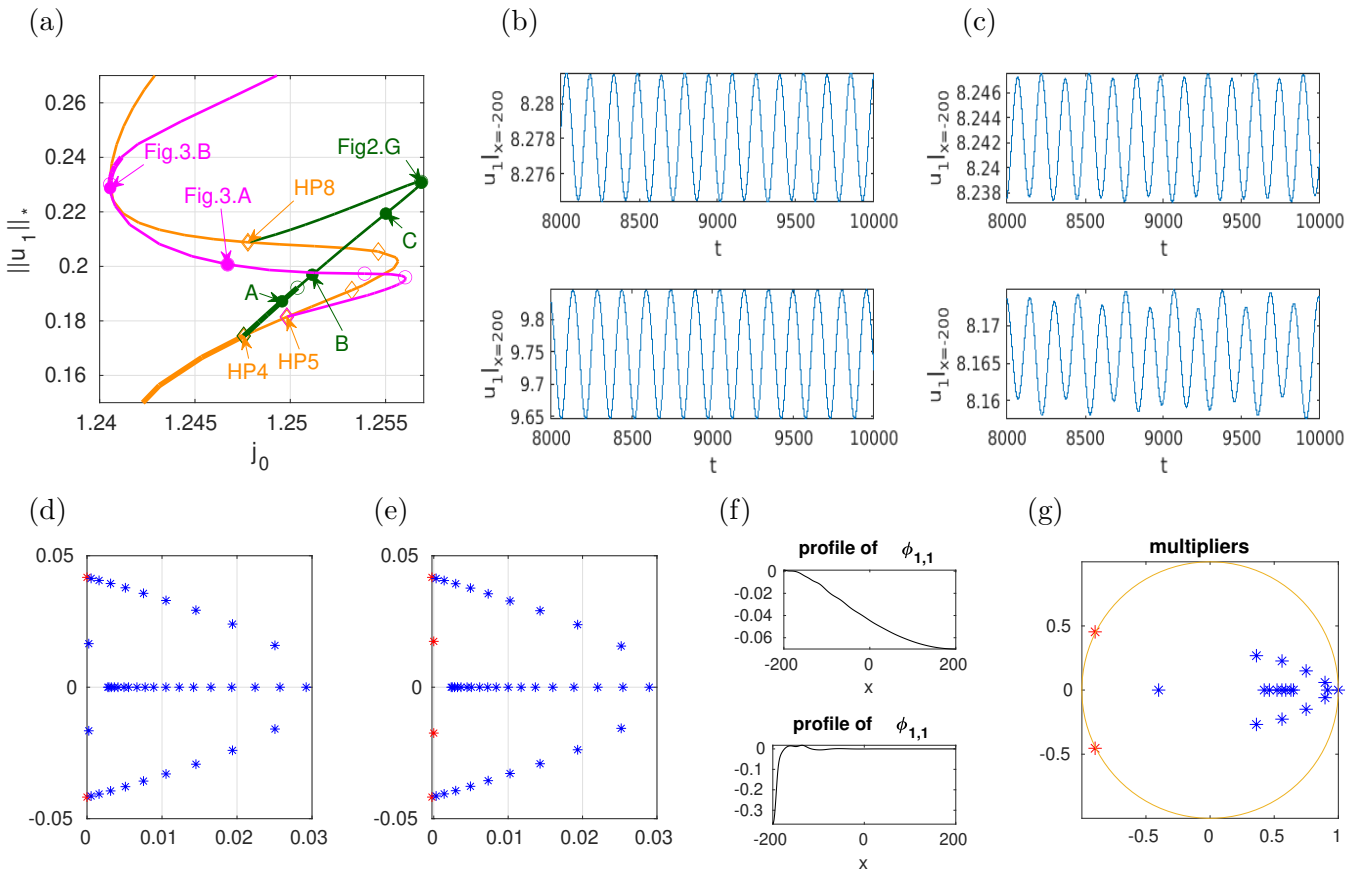

Figure 5: Details of the first green THMM segment, and start of magenta LSW segment. (a) BD with stability indicated by thicker lines. (b) Time series at left and right boundary points from DNS starting at (small perturbation of) A (stable). (c) Time series starting at B (top) and C (bottom), showing a second frequency at the left boundary, with effect growing with increasing j_0 (and negligible at the right boundary). (d,e) Spectra of linearization at HP4 (d) and HP5 (e). (f) Spatial profiles of critical eigenfunction $\phi_{1,1}$ (u_1 component) at HP4 (top) and HP5 (bottom), illustrating the fundamental difference between these two HPs and the bifurcating branches. (g) Floquet multipliers at the torus BP between A and B.

unstable. It follows that in the regime of $j_0 \in (1.24, 1.26)$ we have so far uncovered a rather small number of stable branches, namely H1, some green segments, and a short LSW segment. We therefore turn to the use of DNS to get an idea of the dynamical behavior of (1) in this regime, starting from different ICs. It turns out that this typically yields yet another solution type, namely (irregular) "LSW and Hopf Mixed Modes", LSW-H-MM. However, the first 3 panels in Fig. 6 illustrate known solutions and stabilities: in (a) we start from profile 3.E and go to the branch containing profile 2.G which is stable. In (b) we start near profile 3.B but just below the fold, and the solution collapses to u^* albeit after a long transient. In (c) we illustrate stability of the LSW in 3.B above its first fold (the profile c_2 reveals the presence of the associated small amplitude oscillations at the left boundary).

In panels (d)-(f) we illustrate long time dynamics not directly related to the branches computed by continuation. In (d) we start from the unstable LSW 3.C, which shows three in-phase oscillating troughs. The two left ones evolve into approximately uniform (H type) oscillations, while the third trough deepens and hence the solution transiently resembles ($t \in (3000, 6000)$, say) a H-LSW-MM solution, where the periods of H and the LSW are roughly in 2:1 resonance. However, at larger t the background on the right also starts to oscillate and hence this state turns into a H-LSW-H-MM solution. In (e) we start from the unstable LSW solution 3.G with out-of-phase oscillations of the troughs. Here the solution keeps the general shape of a 3LSW, but the three troughs oscillate in an irregular way. Finally, in (f) we start from the THMM 3.H, and the solution evolves into a mix

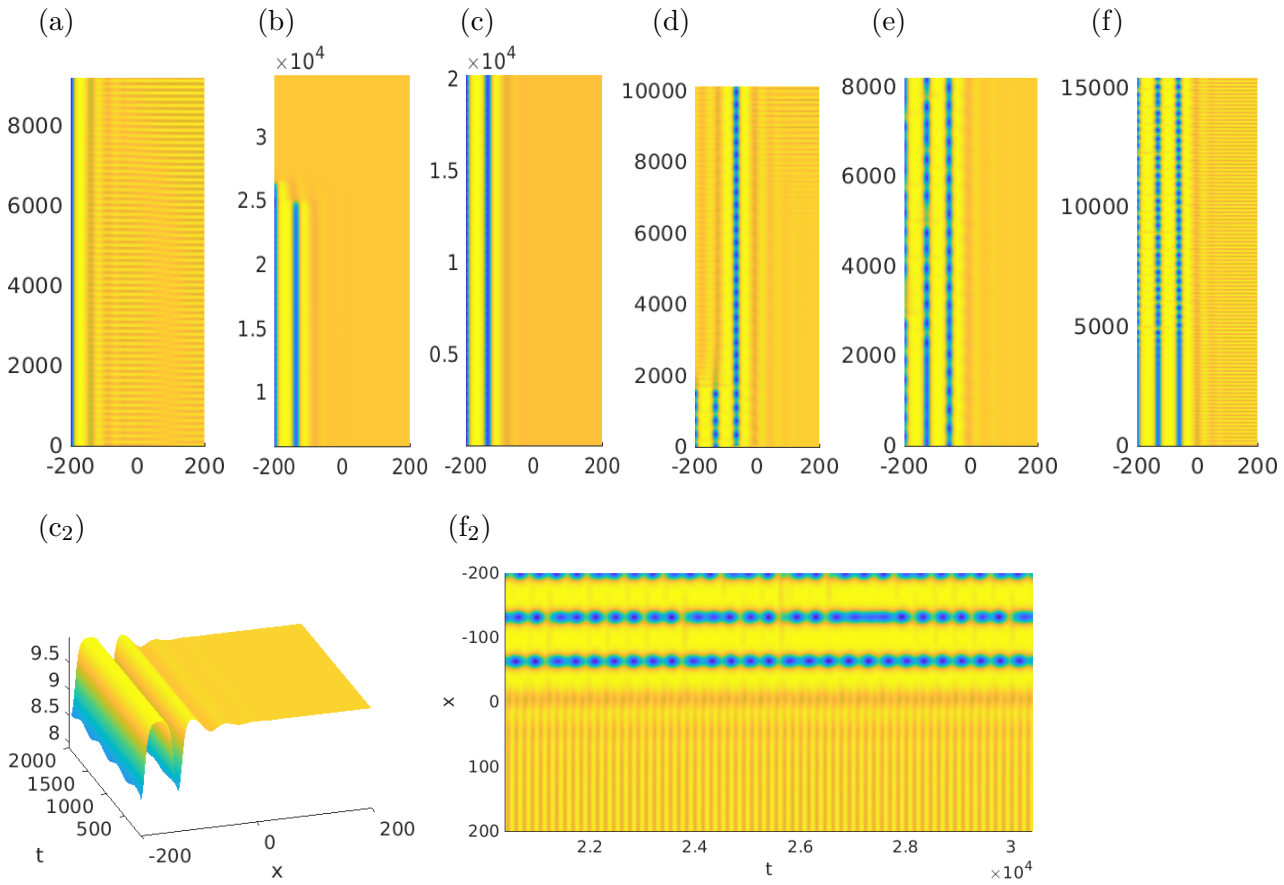

Figure 6: DNS from (small perturbations of) some states in Fig. 3. (a) From point E, the system converges to THMM. (b) From a point shortly before point B, the system converges to u^* after a long transient. (c) From point B, the system returns to B, showing stability of the solution 3.B, see also c_2. (d) From point C, the system develops into a H-LSW-H mixed but apparently non-chaotic mode. (e) From point G, the system develops into an 'irregular' L3SW. (f) From point H, the system develops into a to L3SW-H mixed mode, see also f_2 for details at large t.

of (irregular) LSW with three troughs on the left, and roughly homogeneous (H type) oscillations on the right, i.e., a LSW-H-MM; see panel (f_2) for details of the long time dynamics. Again there is roughly a 2:1 resonance between the H and the LSW with the H oscillation phase at the front ($x \approx 0$) slightly ahead of the phase at $x = 200$. Related coupled breathers have been found in other systems as well, e.g. [AWAN22, AGN24], albeit embedded in a steady homogeneous background.

Remark 3.2 The breathing states shown in Fig. 6(e)-(f) are probably best understood as a system of five (via reflection in $x = -l$) nonlinear oscillators coupled via the intervening "yellow" regions. Such coupling can lead to both synchronized or unsynchronized oscillations depending on its strength. Note that we have only computed solutions of this type where the troughs are located at the domain boundary. Related solutions with a peak at the boundary would lead to an even number of coupled oscillators. ⌋

In Fig. 7 we show the time series of u_1 from Fig. 6(c) and (f), namely u_1 at $x = -200$ (left boundary), and (for (f)) at $x = 0$ (center), and $x = 200$ (right boundary), and their Fourier transforms

$$w^{(j)}(\omega) = \frac{1}{\sqrt{2T}} \int_{t_0}^{t_0+T} \mathrm{e}^{\mathrm{i}\omega t} u_1(t, x_j)\, \mathrm{d}t, \tag{7}$$

where T is the formal period (i.e., the length) of the time series $t \mapsto u_1(t, x_j)$ (technically, we use the properly scaled FFT). In (a) we see the very regular oscillation of the stable LSW. In (c,d), as already

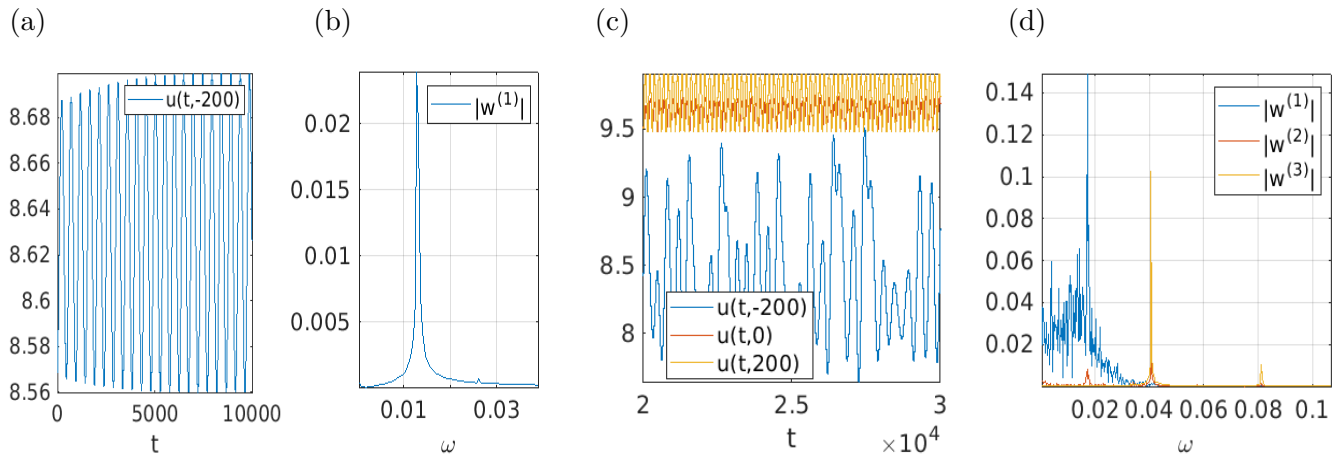

Figure 7: (a) Time series and (b) FFT from Fig. 6(c) at the left boundary, with FFT based on the time interval $t \in [10^4, 2 \cdot 10^4]$. (c),(d) As for (a,b) but with DNS from Fig. 6(f), with time series at $x = -200$ (left boundary), $x = 0$ (center) and $x = 200$ (right boundary), and with FFT based on the time interval $t \in [2 \cdot 10^4, 5 \cdot 10^4]$. The blue time series and broadened FFT correspond to irregular oscillations at $x = -200$. Peaks in (d) are at $\omega = 0.0171$ (blue, "period" $T = 367.65$), and $\omega = 0.0409$ (orange, $T = 153.65$), giving a frequency ratio 0.418. The red (center) time series shows contributions from both frequencies.

obvious from Fig. 6(f), the troughs oscillate with *very roughly* twice the period of the background oscillations, but irregularly. From the FFT, the period ratio is 2.3929. At $x = 0$ we (naturally) have contributions from both.

To shed more light on the interface between LSS (or LSW) in one part of the domain, and the oscillations in the rest and to otherwise assess the genericity of dynamics shown in Fig. 6(d)-(f), we show in Fig. 8 the same problem on twice the domain $(-400, 400)$. In panel (a) we show a partial BD, with the same color codes as in Fig. 2. Before the primary Turing T1 branch (blue), we now have 6 Hopf branches bifurcating from u^* due to the denser sidebands, and we show H1 and H3 in brown. The orange LSS snake bifurcates from T1, but unlike Fig. 3 we now omit the PO branches bifurcating from it. We do this for three reasons: there are many more HPs (102 on the full branch), the computation of the bifurcating POs becomes more expensive, and, most importantly, typical dynamics can be illustrated by starting directly from points on the orange snake as indicated.

In panel (b) we start at the beginning of the snake and after a long transient converge to the uniform oscillation H1. In panel (c) we show an analogue of Fig. 6(f): starting near the small amplitude LSS at point C, the solution first resembles a LSW ($t \in (5000, 10000)$, say), before H1 develops on the right and the solution develops into a LSW-H-MM. See panel (c_2) for the late time dynamics, which shows more clearly than Fig. 6(f_2) that the background oscillations are low wave number waves traveling towards the interface (here at $x \approx -300$). Panel (d) shows convergence to a LSW, while (e) shows the emergence of an (irregular) LSW-H mix. This last case is in fact the typical behavior for generic ICs for which we do not get convergence to H1 or a steady state.

Remark 3.3 Interfaces such as those shown in Fig. 8(c2) or Fig. 10(B) have been seen before [TMB+13, APR23] but their understanding remains incomplete. The fact that one observes slowly traveling waves instead of the expected uniform oscillation could be related to the fact that in region C several sidebands of H1 are unstable, but we consider this unlikely since all the resulting branches are expected to be unstable. Instead, we believe that the observed nonzero wave number arises due a nontrivial effective BC at the interface between the LSS and the background oscillation. Since this BC remain unknown we have not been able to confirm this hypothesis. The traveling states observed and studied in [DWLDB96] have a different origin related to subharmonic resonance that is responsible for the finite phase speed of these oscillations. ⌋

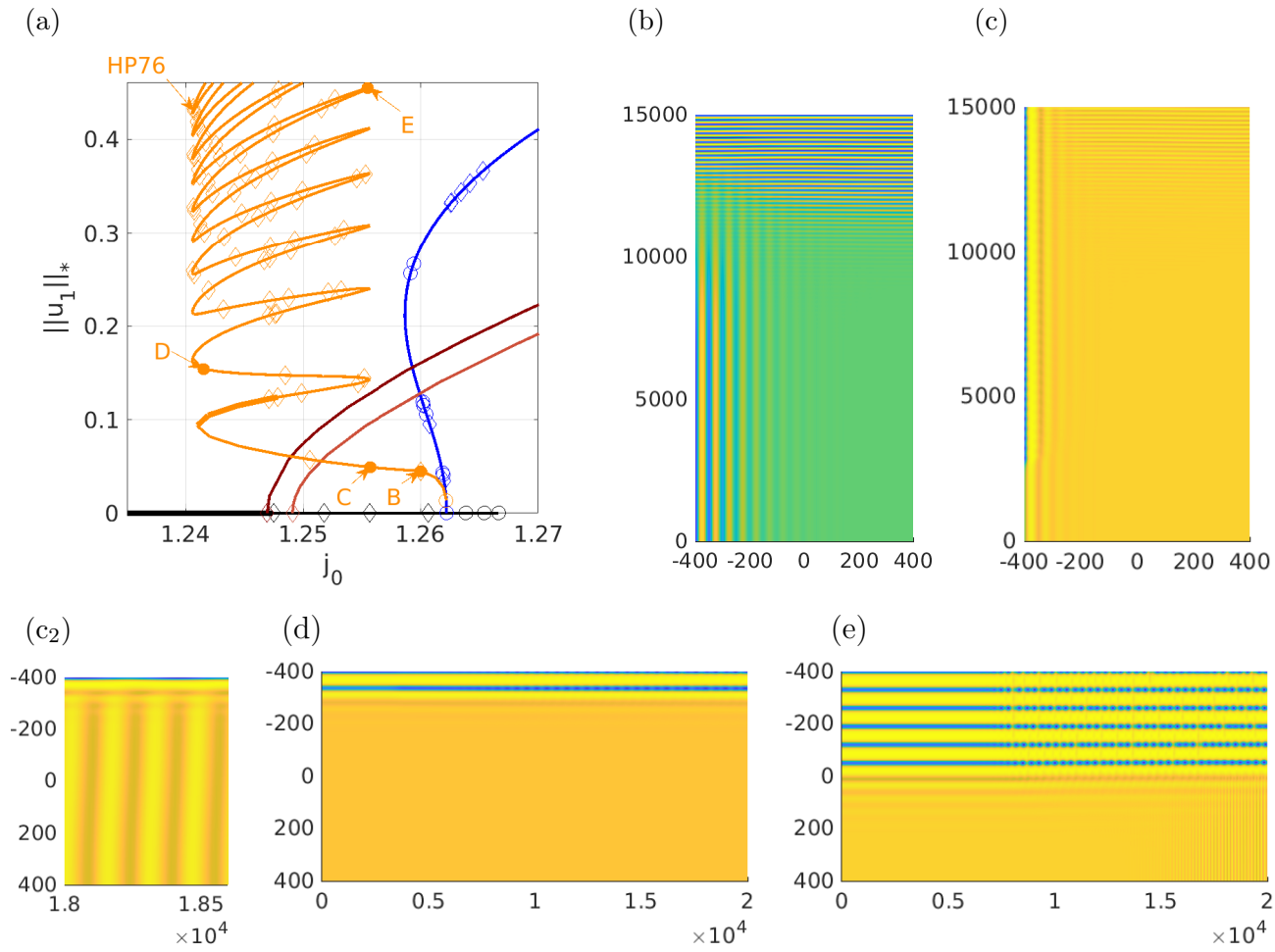

Figure 8: (a) Partial BD on a larger domain, $\Omega = (-400, 400)$, with $(\alpha, D, \tau) = (0.035, 6.5, 0.05)$. (b)-(e) Selected DNS from (perturbations of) solutions marked in (a). Convergence to H1 in (b), to LSW-H mix in (c) with late time zoom in (c_2), to (irregular) LSW (d), and to LSW-H-MM (e).

3.1.4 Zipping/unzipping in D

We now return to the continuation setting and want to study how the organization of the THMM and LSW branches depends on parameters. For this purpose, our main tools are fold-point continuation (FPC) and Hopf-point continuation (HPC) of the folds and HPs on the orange LSS snake.

Figure 9(a) shows HPC of HP3 (red) and HP4 (green) from LSS from Fig. 2. An important feature is that as D decreases the two HPs collide at a FP, and do so with identical frequencies ω; the same happens for other THMM HP pairs. For example, HP10 and HP11 (connected by the next green branch in Fig. 3) collide at a right fold when increasing D. See [AKNU24, Remark III.1a)] for further comments on these collisions as codimension-2 phenomenon, even though one would at first expect codimension-4. Put differently, to continue the THMM HPs in D we can just continue HP3 in D; this then repeatedly moves up through folds, as illustrated in panel (b) together with FPC of FP1 and FP2 on LSS. Because all the left (resp. right) folds on LSS in Fig. 2 are well aligned with FP1 and FP2, the continuation of FP1 and FP2 gives a good approximation of the snaking region of LSS as a function of D, which becomes exponentially thin [CK09] as $D \searrow D_c \approx 5.5$. The HPC is confined between the orange FPC lines, but only approximately so because after moving up through one fold on the right, say, the HP must occur before the next left fold.

We next turn to the HP B shown in Fig. 9(b) at $D \approx 6.267$. If we compare the number of HPs at the starting value $D = 6.5$ (Fig. 2) with that at location B with $D \approx 6.267$, we see that several HPs from the original LSS snake at $D = 6.5$ no longer exist at B. This is a consequence of the leftward

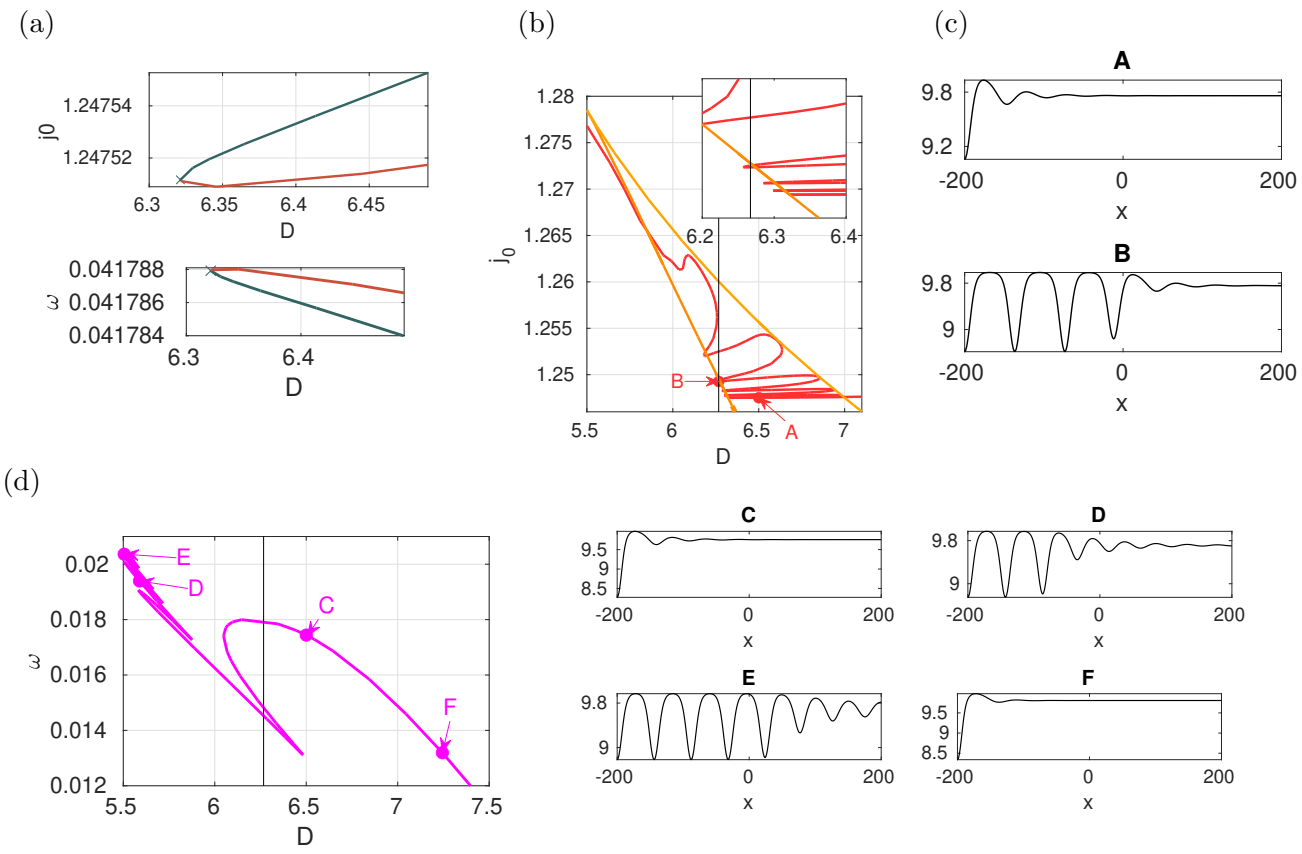

Figure 9: (a) HPC of HP3 (red) and HP4 (green) on LSS from Fig. 2. (b) Further continuation of HP3 (red), and FPC of FP1 and FP2 on LSS. (c) Sample profiles from (b). (d) HPC of LSW-HP on LSS (magenta branch), explaining why the LSW branch is broken into three segments when D=6.267 (vertical line), see Fig. 10.

slant of the HPC in Fig. 9. Since these HPs are responsible for the short THMM connections (Fig. 3) this implies that the associated branches must have recombined: this is the mechanism that turns a stack of short THMM into a long THMM snake by the time $D \approx 6.267$. This zipping up process does not qualitatively affect the behavior of the short TH2MMs (Fig. 3, profile E) that are still present at B because they are generated by distinct HPs with distinct frequencies ω and eigenfunctions.

It follows that Fig. 9(b) provides an important insight into the (partial) BD for $D = 6.267$ shown in Fig. 10 computed by starting at point B in Fig. 9(b) and varying j_0 in either direction. Starting at HP1 (see figure) and proceeding in the direction of decreasing j_0 we obtain the upper part of the LSS snake (orange), on which we have further HPs, with HP2 and HP3 corresponding to the two additional intersections of $D = 6.267$ with the red curve in Fig. 9(b) above location B (see inset). HP1 itself marks the beginning of the long THMM snake (red) that extends to lower norm before heading out towards large j_0 past location B (Fig. 10). At HP2 a (short) "out-of-phase" LSW snake starts (violet, profiles C and D), while HP3 corresponds to the start of the short THMM (green, profile E) that terminates back on LSS at HP7. Going from HP1 in the other direction (initially increasing j_0), we generate the lower part of the orange lSS snake, with altogether 10 HPs on it, starting counting at HP1 again, and from these HPs LSW (violet, profiles F and G) and TH2MMs bifurcate, but no further THMM, because these have zipped up into the red snake.

Thus, while the THMM segments have almost fully zipped up at this lower $D = 6.267$ compared to $D = 6.5$ in Fig. 2, the LSW snake in Fig. 2 (magenta) has partially *unzipped* into the violet segments in Fig. 10. This can also be explained using Fig. 9(d): While at the initial $D = 6.5$ we have only one HP of LSW type (sample profile C), there are three such points at $D = 6.267$, with

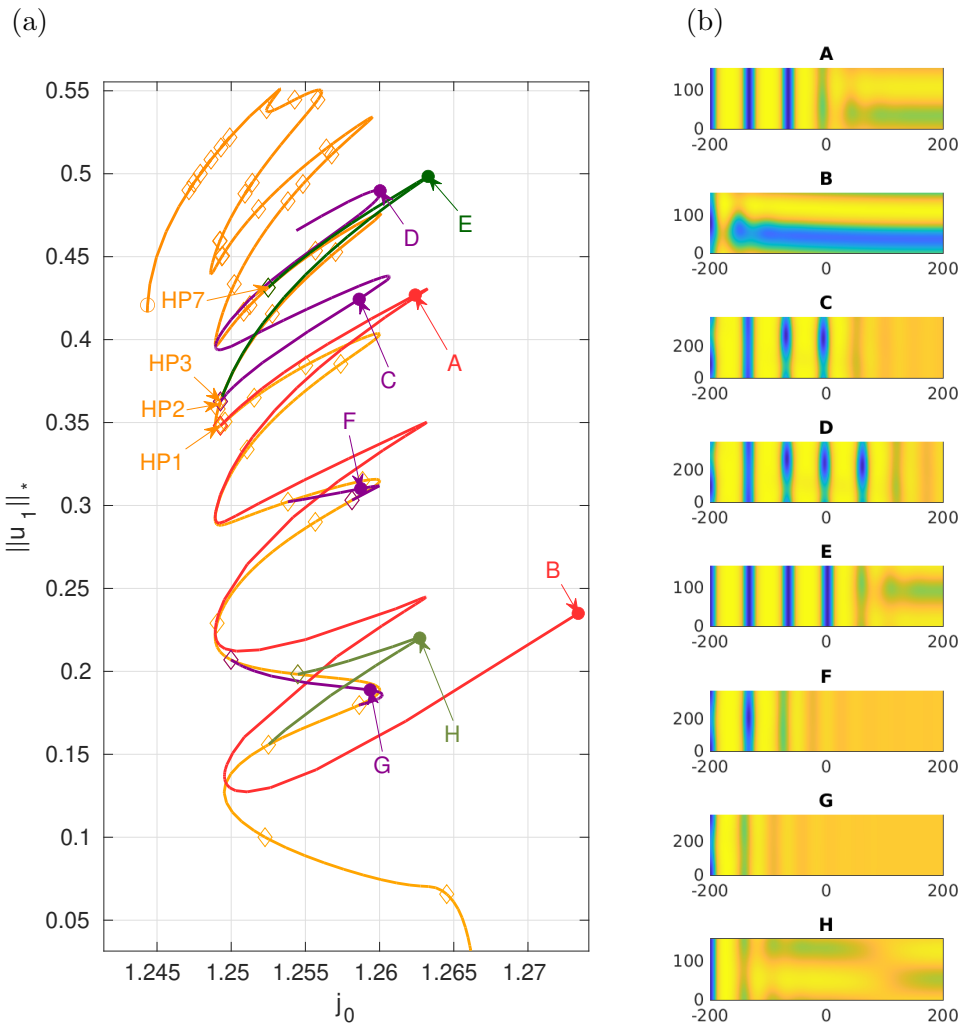

Figure 10: Back to continuation in j_0 from Fig. 9(b), point B ($D = 6.267$). Some of the short dark green THMM segments near the bottom have zipped up into a THMM snake (red) that extends to large j_0. Some short lighter green TH2MM segments remain, profile H (the integer j in THjMM refers to the background wave number). Conversely, the former magenta LSW snake has unzipped into short LSW connections, e.g., profiles F and G. The top of the LSS snake still features short THMM (dark green) segments, profile E, and "mixed LSW" segments and snakes (violet), profiles C and D. Beyond location D, the different trough oscillations go out of synchrony and the solutions cease to be periodic in time and can no longer be followed.

the two new ones responsible for the breakup of the LSW snake into two short segments (profiles F and G in Fig. 10). The further HPC in Fig. 9(d) to lower D shows that the LSW HPs move up the LSS snake where the corresponding solution profiles fill the domain (profiles D and E).

A similar zipping/unzipping also occurs using the parameter τ (not shown) but fails when α is varied instead.

3.2 Vicinity of C2TH$_2$

3.2.1 Basic branches at $D = 6.5$

The behavior of (1) near C2TH$_2$ with respect to the primary Hopf and Turing branches mirrors to some extent that near C2TH$_1$, with the main difference being that the Hopf branches now bifurcate subcritically, i.e., towards larger j_0; see Fig. 11 for an overview at $(\alpha, D, \tau) = (0.034, 6.5, 0.05)$.

The figure again shows a pair of primary Hopf branches, H1 and H3, in shades of red, the first

Turing branch T1 in blue, and the first LSS snake bifurcating from T1 in orange. The violet branch TH1MM bifurcates from HP3 on LSS and makes a long excursion to large amplitude where it enters a snaking region (Fig. 12), characterized by the usual stability changes at the folds (profiles D and E), before reconnecting to LSS in HP12. Note that H1 is stable after its fold, while the stability of the LSS follows the classical picture [BK07] despite the fact that T1 corresponds to the fourth unstable mode of u^*. This is because the three Hopf instabilities inherited by this state are eliminated one by one via three secondary HPs along the lowest part of the LSS branch (see Fig. 11(a), inset). The THMM states (violet) can also be stable, in particular in the snaking region located at the top of the BD (see Fig. 12, as well as Fig. 20(c) and the movies).

In Fig. 13 we zoom into the orange LSS snake and in green show three THMM type connections bifurcating from LSS, namely HP4 to HP5, HP6 to HP7, and HP8 to HP9. In contrast to the "short" THMM segments in Fig. 3, these are "long" connections, generally showing $O(1)$ oscillations away from the HPs. In contrast to Fig. 3, there are *only* THMM HPs on the orange snake (there are no LSW HPs), and consequently fewer HPs (1 to 12) in total. A further important difference from Fig. 3 is the different connection structure between HPs, which becomes apparent from HPC and PO continuation in the parameter D as discussed next.

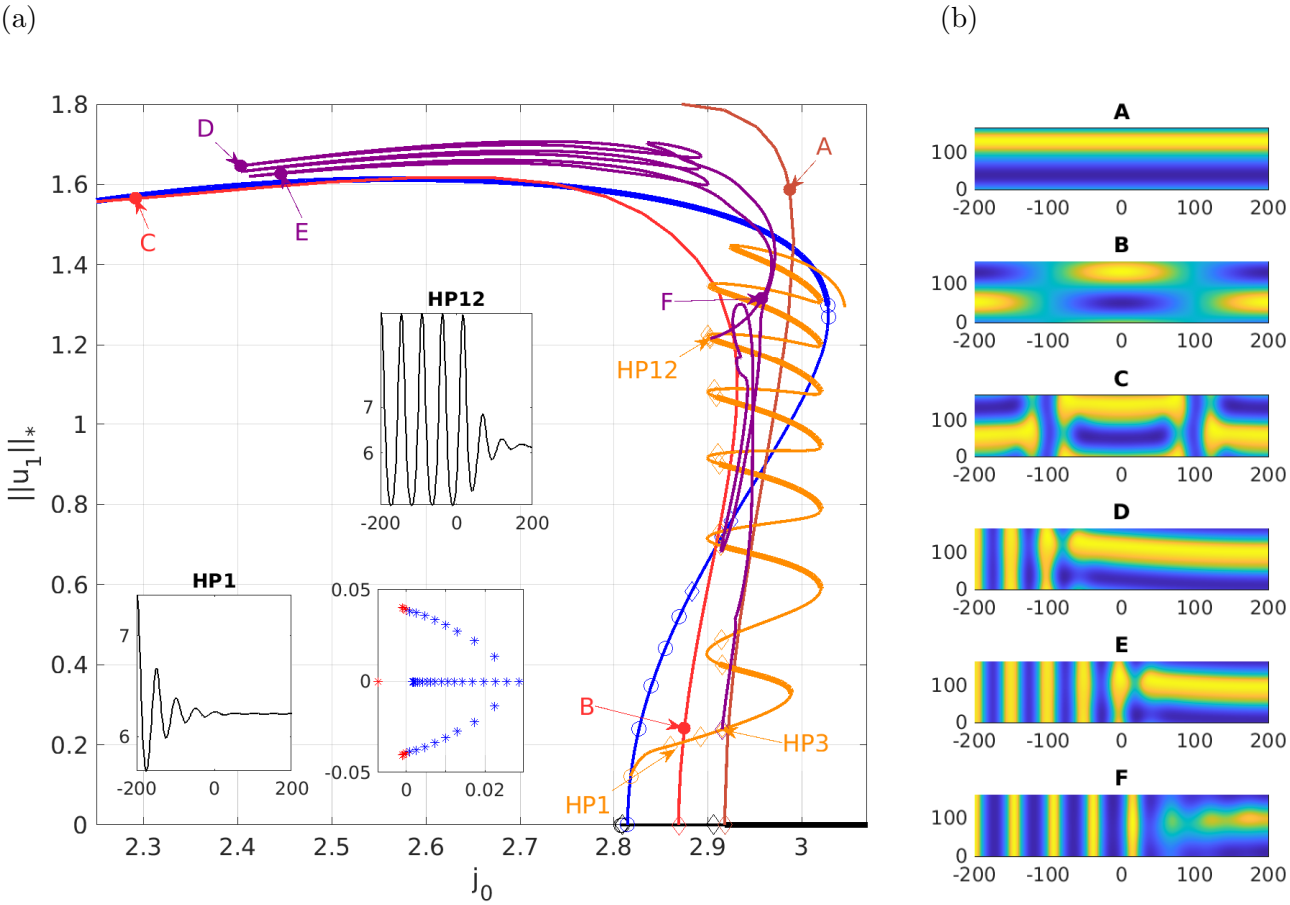

Figure 11: (a) Partial BD near C2TH$_2$, i.e., $(\alpha, D, \tau) = (0.034, 6.5, 0.05)$, showing a pair of subcritical Hopf branches (shades of red) and a subcritical Turing branch (blue), with (b) sample solution profiles at locations indicated in (a). A TH1MM branch of time-periodic mixed modes (violet) is also shown and exhibits classical snaking near the top. See Fig. 12 for a zoom of the upper part of the violet branch and Fig. 13 for a zoom of the orange snake and solutions that bifurcate from it. For completeness, the insets in (a) show the solution profiles at HP1 and HP12 and the associated spectrum of the linearization at HP1, yielding two Hopf eigenvalues and five unstable eigenvalues (red).

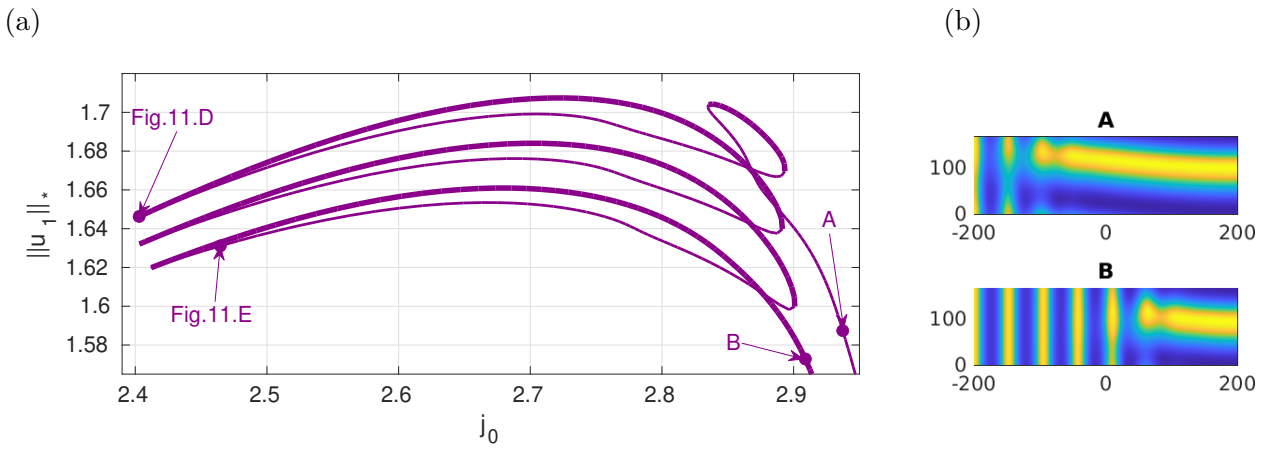

Figure 12: (a) Zoom into the top of the violet branch in Fig. 11, showing typical snaking behavior with change of stability at the folds. Thick (thin) lines indicate stable (unstable) branches. (b) Sample solution profiles at two additional locations indicated in (a) showing a solution before entering the snaking region and again after exiting the snaking region.

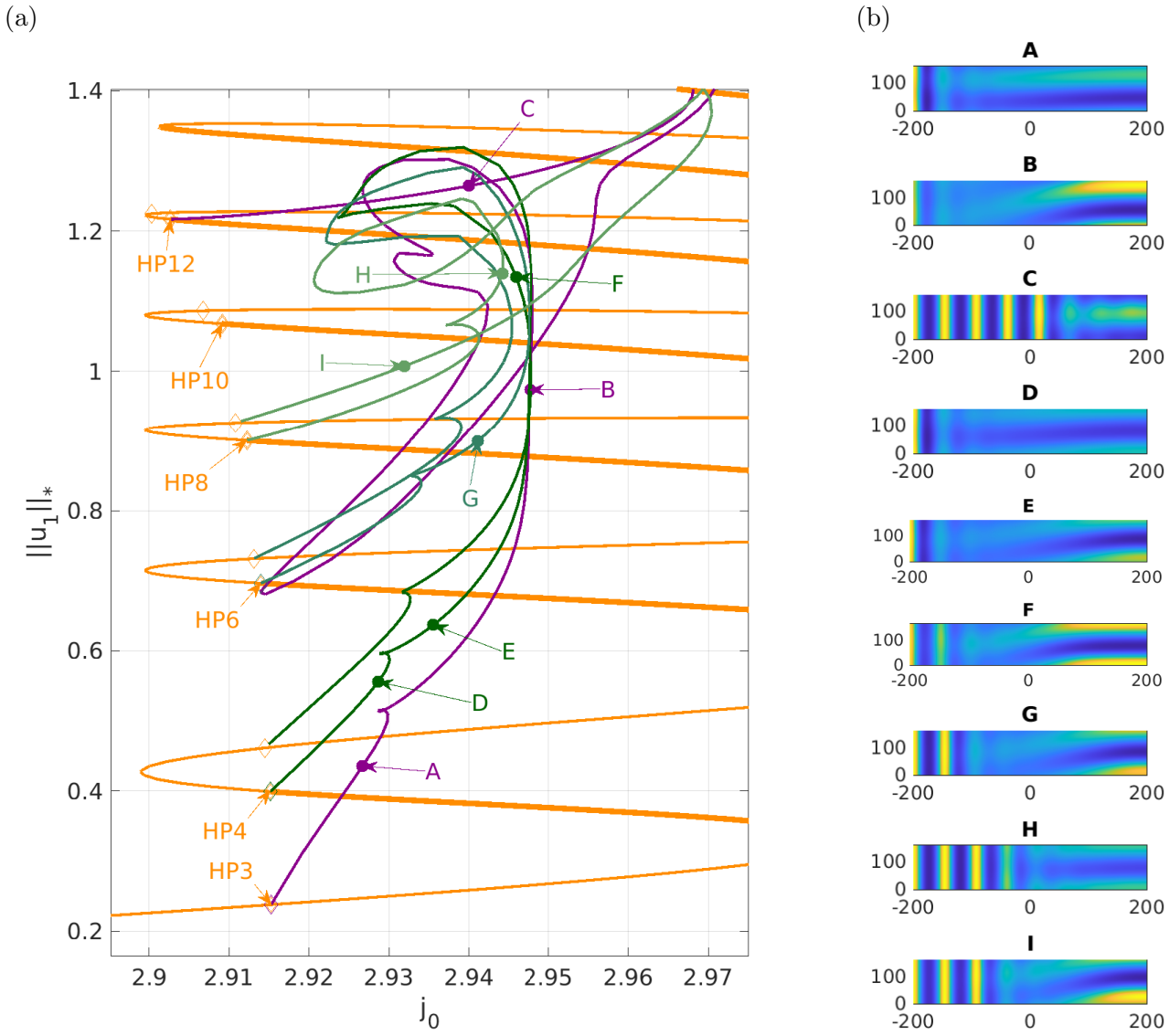

Figure 13: (a) Zoom into BD in Fig. 11 with (b) sample solution profiles at locations indicated in (a). Solutions originating in HP4, HP6 and HP8 are referred to as PO4, PO6 and PO8, respectively. Profiles D and F on PO4 are used for PO continuation in D to illustrate reconnection phenomena near $C2TH_2$, and the detachment of isolas as D varies.

The little cusp near locations A or D suggests that at some other D their "analogs" may lie on the same branch, which lets us suspect that upon continuation in D the "long" connections such as the violet (between HP3 and HP12) and some green ones (e.g., between HP4 and HP5) may reconnect into short connections (e.g., between HP3 and HP4) and isolas (e.g., parts of the violet branch containing B, and of the dark green branch containing E). Naturally, these reconnections cannot be "local phenomena", i.e., the "remainder" of the green branch in Fig. 13 connecting back to HP5 must also reconnect at the same D. Thus, to trace and understand this rather complicated process, we need to complement HPC in D on the orange snake with PO continuation (POC) in D of, e.g., profiles D and F from Fig. 13.

3.2.2 HPC and POC in D

Figure 14 shows HPC of HP3 on the orange LSS snake from Fig. 13, together with FPC of FP2 (1st left fold) and FPC of FP3 (2nd right fold, which is at larger j_0 and hence is on the *left* in Fig. 14). This behavior looks qualitatively similar to that in Fig. 9. Starting in the direction of decreasing D, HP3 first collides with HP4 at the first right fold, and continues as HP4. Further HPC is confined between the two FPCs, and the HP ascends the orange snake, adding Turing wavelengths on the left. In the other direction, increasing D, HP3 leaves the range given by the FPCs.

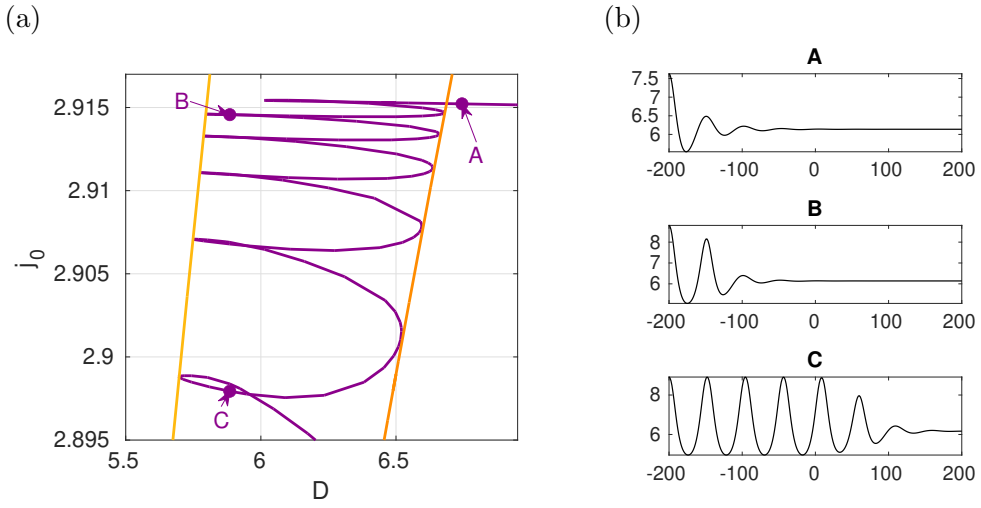

Figure 14: (a) HPC for HP3 on orange snake from Fig.11 and Fig.13, and FPC for FP2 (right, dark orange) and FP3 (left, light orange) together with (b) sample profiles at locations indicated in (a).

From this, we may first of all conclude that for $D > 6.7$ (outside the FPC range) the THMM HPs HP4–HP12 have disappeared, implying reconnection phenomena with increasing D to, e.g., point A of the HPC. Similarly, since the HPC slants to the left with decreasing D, one finds that at smaller D (near FPC3) the HPs at the bottom of the LSS snake from Fig. 13 (other than HP1-HP3) are the first to disappear, again yielding reconnections. However, these are different and more complicated than the reconnections (the zipping up) of the THMM branches in Fig. 10. For instance, on decreasing D we find a breakup of the long THMM branches into isolas and short THMM branches connecting HPs that subsequently collide, and in these collisions the connecting short THMM branches disappear, leaving behind the disconnected THMM isolas. See Figs. 18 and 19 below for further illustration of this process.

In Fig. 15 we return to continuation in j_0 starting at point A in Fig. 14 with D kept fixed at $D = D_A \approx 6.744$.[5] As predicted, HP4-HP12 from Fig. 13 have disappeared. Consequently, the

[5] We first obtain the (new) orange LSS snake, which we continue in both directions from the initial $j_0 \approx 2.915$. Towards the bottom we locate the three remaining HPs, HP3–HP1, in reverse order, and from these we compute the

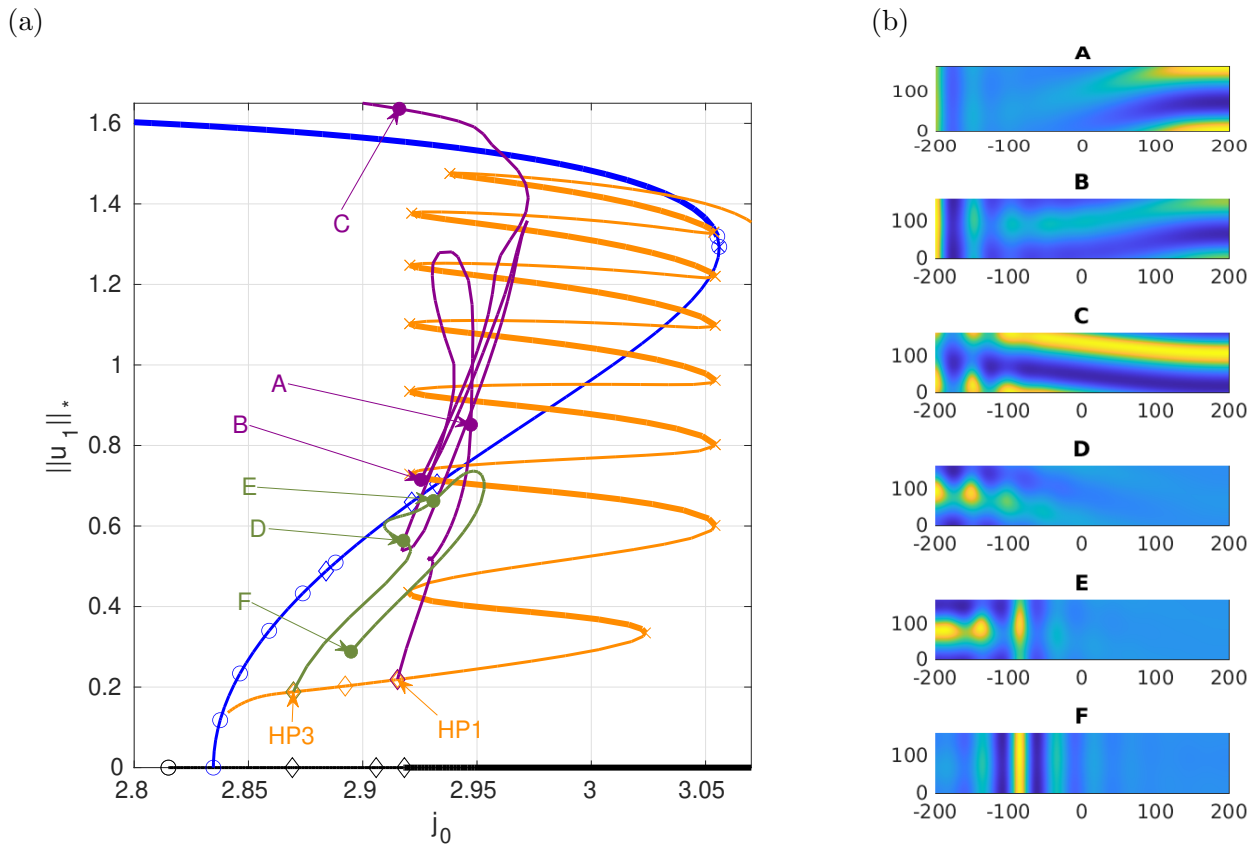

Figure 15: (a) Return to continuation in j_0 from location A in Fig. 14 with D fixed at $D_A = 6.744$ with (b) sample solution profiles at locations indicated in (a). All HPs on the orange LSS snake have vanished except for HP1-HP3 (numbers reversed now) and the violet branch with sample profiles A-C now extends to low j_0, and all other THMM branches from Fig. 11 detach as isolas, see Fig. 18.

former TH1MM branch from Fig. 13 can no longer connect to LSS, and instead it continues to larger and larger amplitude (and smaller j_0), see profiles A-C. For completeness, we also show HP3 from LSS, which now connects to different LSS branch, profiles D-F. After reflection in $l = -200$ we see that this is a two-pulse snaking branch [BK09]. An immediate question is what happened to the long THMM branches PO4, PO6 and PO8 in Fig. 13, arising from HP4, HP6 and HP8, respectively, and containing large amplitude oscillations. These cannot reconnect into a THMM snake as their HP base points on LSS collide and disappear, because, e.g., PO6 does *not* pass close to the HPs HP4 and HP5 which are connected by PO4. Hence, they must detach from the LSS snake as isolas, as illustrated in Fig. 18 below. Thus the resulting isolas are all distinct and simultaneously present.

In Fig. 16 we show the results from continuation in j_0, this time starting from location B in Fig. 14 with D kept fixed at $D_B \approx 5.885$. From Fig. 14 it follows that here *all* THMM HPs from Fig. 13 still exist (except for HP3), but some reconnections of THMM branches nevertheless occurred as the THMM HPs moved to the right. Specifically, HP1 and HP1b (formerly HP5 and HP6, unconnected in Fig. 13) are now connected by a short segment, profile A, while HP8 and HP9 (formerly HP9 and HP10, unconnected in Fig. 13) are now connected by another short segment, profile B. This is only possible, however, if the "remainders" of the former long connections also reconnect, and below we show that this generally results in the formation of isolas (not shown in Fig. 16, as this figure is strictly generated by continuation and bifurcation in j_0). Note also that the former HP12 (now HP18) has lost its partner (HP3 in Fig. 11), and indeed the branch bifurcating from HP18, profile F, now extends monotonically to smaller j_0.

violet and green PO branches by branch switching. Additionally we compute the black trivial branch and the blue primary Turing branch by starting the continuation in j_0 at $u = u^*$ and $D = D_A$, $j_0 = 2.95$.

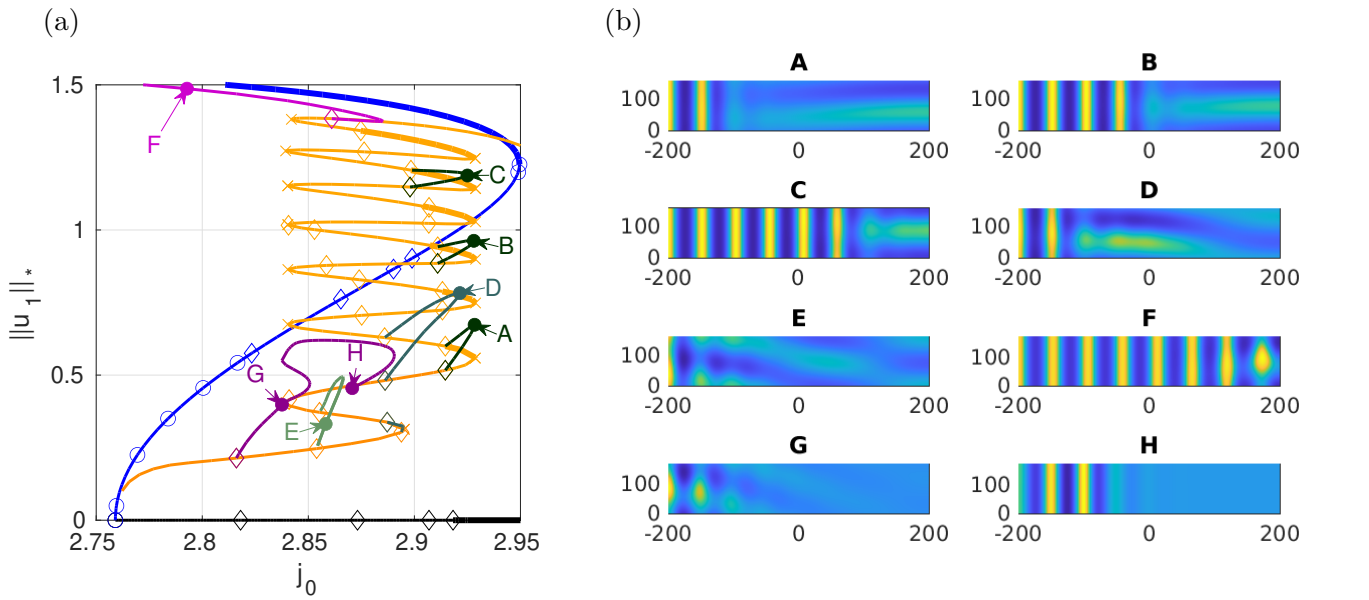

Figure 16: (a) Return to continuation in j_0 from location B in Fig. 14 with D fixed at $D_B = 5.885$ with (b) sample solution profiles at locations indicated in (a). The long segments have broken up into short segments and isolas (not shown, see Fig. 18) while other short connections of type TH$_j$MM with $j = 2$ or $j = 3$ have moved in (profiles E, F); there is an additional PO branch (violet, profiles G, H) connecting LSS with itself.

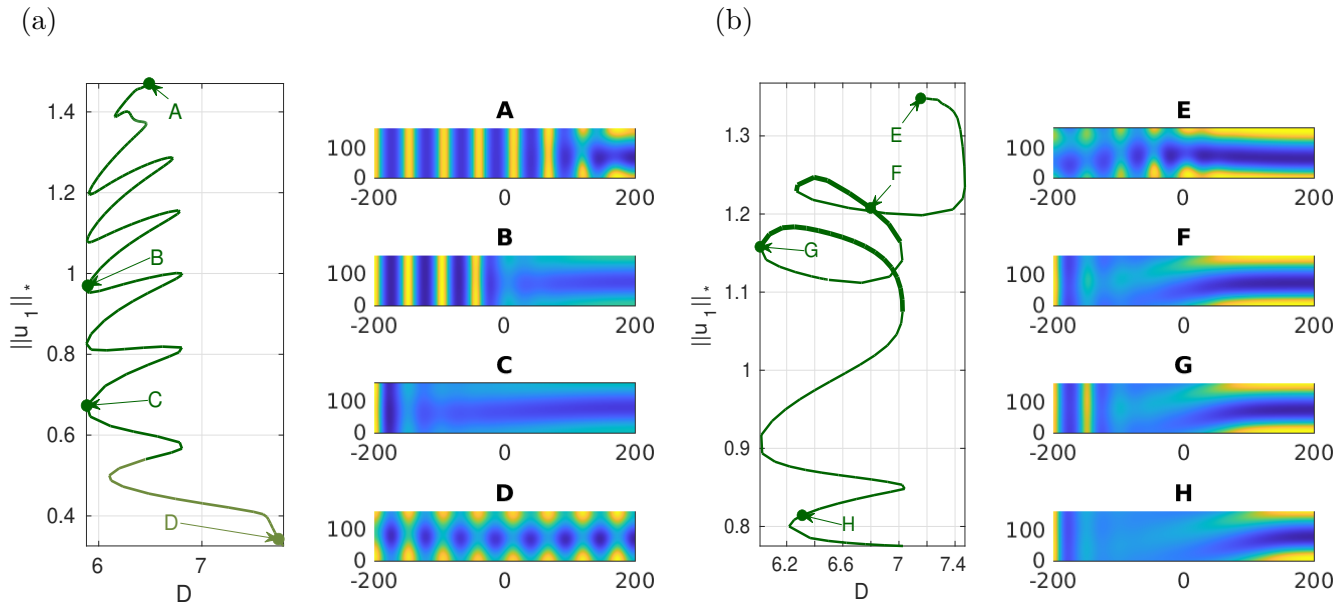

Figure 17: PO continuation in D from (a) location D in Fig. 13 resulting in a nice THMM snake that appears to bifurcate from a SW at the bottom right (profile D) and (b) location F in Fig. 13 resulting in more complex behavior owing to large amplitude oscillations in the background. The change in color shade indicates the start of POC. Solution C at $D = 5.88$ is used in Fig. 18 to generate the "short connection", while F at $D = 6.8$ and G at $D = 6$ both lead to isolas in Fig. 18. See Fig. 19 for details of the reconnections when returning to continuation in j_0 from points *near* C. All POs in (a) unstable, some segments in (b) stable as indicated by thicker lines.

To obtain starting points for the expected isolas omitted from Figs. 15 and 16, we directly continue in Fig. 17 two POs from branch PO4 in Fig. 13 in the parameter D. In some cases, such as panel (a), this yields a snaking THMM branch in which a Turing wavelength is added to the Turing part of the solution at every second fold, as in [TMB$^+$13], cf. Fig. 3 for similar behavior near C2TH$_1$.

Moreover, in this case the origin of the THMM snake can be traced to a bifurcation from a SW, see profile D. However, in other cases such as that shown in panel (b), we do not obtain a clean snake, apparently a consequence of the large amplitude oscillations in the background.

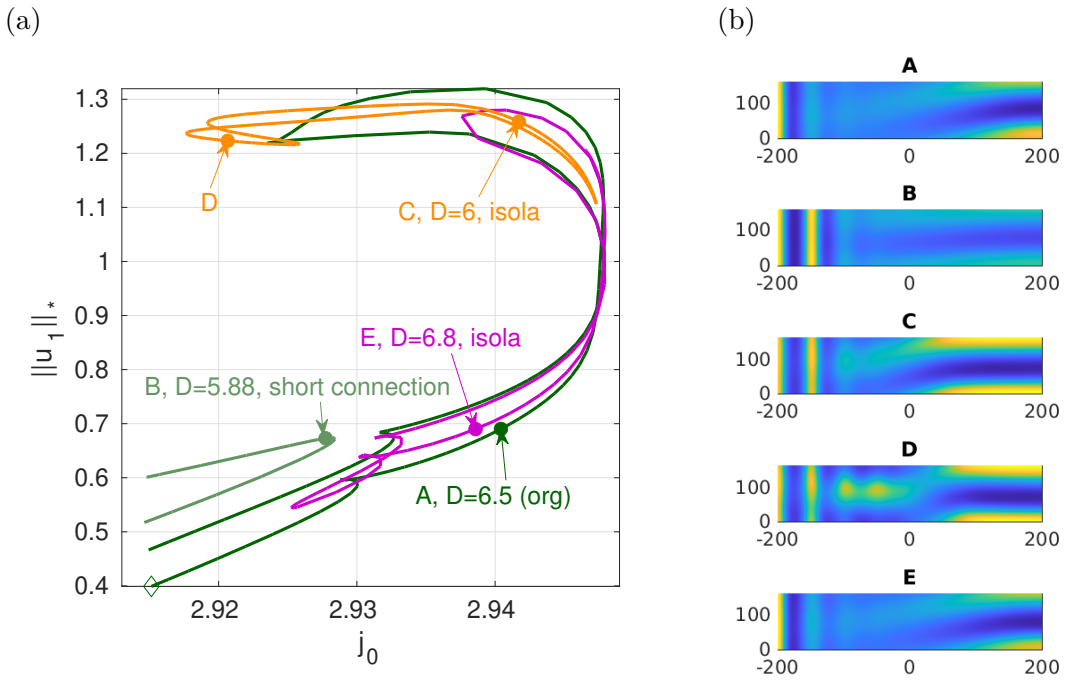

Figure 18: (a) BD of branches at different D with (b) sample solution profiles at locations indicated in (a). Dark green: long original ($D = 6.5$) connection between HP4 and HP5 in Fig. 13. At smaller D this breaks up into an isola (orange) and short connection (light green), computed here a slightly different values of D. At larger D the branch detaches becoming an isola (violet). The corresponding branches are omitted from Figs. 16 and 15, respectively.

More importantly, we can use these results to return to continuation in j_0 at selected points in Fig. 17, and we give an overview of the results obtained in Fig. 18. In addition, Fig. 19 shows the successive breakup of the long connection as the parameter D decreases, in other words, it shows how the system transitions from the case with long PO connections shown in Fig. 15 at larger D (violet) to that shown in Fig. 16 at lower D with short THMM segments (green). The figure shows that the transition occurs in two stages. First, the long connection splits into an upper isola and a semilong connection to LSS. This is followed at slightly lower D by a further breakup, generating a figure-eight isola and one of the shorter segments visible in Fig. 16. Both of these isolas subsequently shrink to a point and both vanish near $D = 5.924$. Figure-eight isolas are generic structures in this type of problem [BKL+09].

3.2.3 DNS

In Fig. 20 we show the results of DNS from some of the states in Fig. 13. We start in (a) from a small amplitude THMM and obtain slow convergence to H1. Here slow means that dynamics similar to H1 is reached at around $t = 5000$, but the phase at the left boundary $x = -200$ is slightly ahead of that at the right boundary $x = 200$, and the subsequent alignment is a very slow process, see the associated time series. In (b) we have a very long transient (up to $t = 35000$) in which we have smaller (and phase-shifted) oscillations near $x = -200$ as compared to $x = 200$, but the oscillations at $x = -200$ eventually start to grow and the phase adjusts yielding convergence to H1. In (c) we see convergence to a stable THMM, while in (d) H1 slowly invades the LSS on the left ($x = -200$) in a stick–slip fashion, generating "H1 with a phase gradient" around $t = 10000$, followed by an even

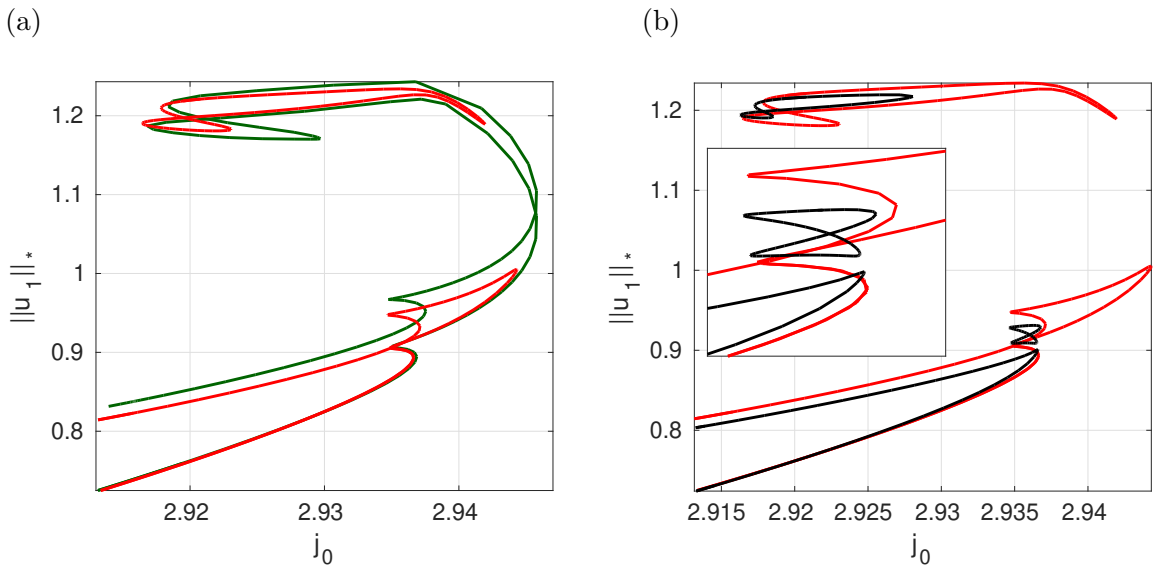

Figure 19: (a) Details of the breakup of the long connection into a large amplitude isola and a semilong connection: $D = 6.047$ (green) vs $D = 5.979$ (red) chosen near point C in Fig. 18(a). (b) Second breakup, this time of the semilong connection, into a shorter segment and butterfly (a figure-eight isola): $D = 5.979$ (red) vs $D = 5.93$ (black). Upon further decrease in D the upper and lower black isolas shrink and both vanish near $D = 5.924$, leaving the short segment only.

slower alignment of the phases. These calculations illustrate some of the possibilities for dynamics at one fixed set of parameter values, and the two main conclusions from these (and further DNS not shown) are that while

- strong multi-stability of different steady and time-periodic patterns is present in this parameter regime,
- the spatially homogeneous PO H1 plays a dominant role in a large parameter range, although its realization may become visible after very long transients only.

4 Discussion

We revisited a two-component reaction-diffusion model of charge transport in a semiconductor (the SECO model) studied in [MDWBS97]. This model is known to exhibit two codimension-2 points corresponding to the simultaneous onset of Turing and Hopf bifurcations of a homogeneous base state, C2TH$_1$ and C2TH$_2$, as shown in Fig. 1(a). The vicinity of higher codimension points always represents an interesting and important parameter choice, since such points serve as organizing centers for nearby dynamics. The SECO model is no exception. In the model the interaction of Turing and Hopf instabilities leads to strong multistability of different patterns. The primary bifurcations are to pure Hopf branches (spatial wave number $k = 0$, and sidebands), and pure Turing branches ($k = k_c = O(1)$, and sidebands). The Hopf branches are supercritical near C2TH$_1$ but subcritical near C2TH$_1$2 while the Turing branches are subcritical in both cases. These facts suggest that a variety of spatially localized states, both steady and time-periodic, are present in the vicinity of these points, and our interest focused on the properties of these states, particularly those of time-periodic localized states. As is well known secondary bifurcations from subcritical Turing branches generate snaking LSS branches [BK07], which in general contain tertiary bifurcations to time-periodic LSS-Hopf mixed branches or THMM branches that are of particular interest in this work. These are of two broad types: Those that lead to periodic breathing of LSS and those that take the form of LSS embedded on a uniformly oscillating background. Some details of these tertiary bifurcations are quite different near C2TH$_1$ and near C2TH$_2$.

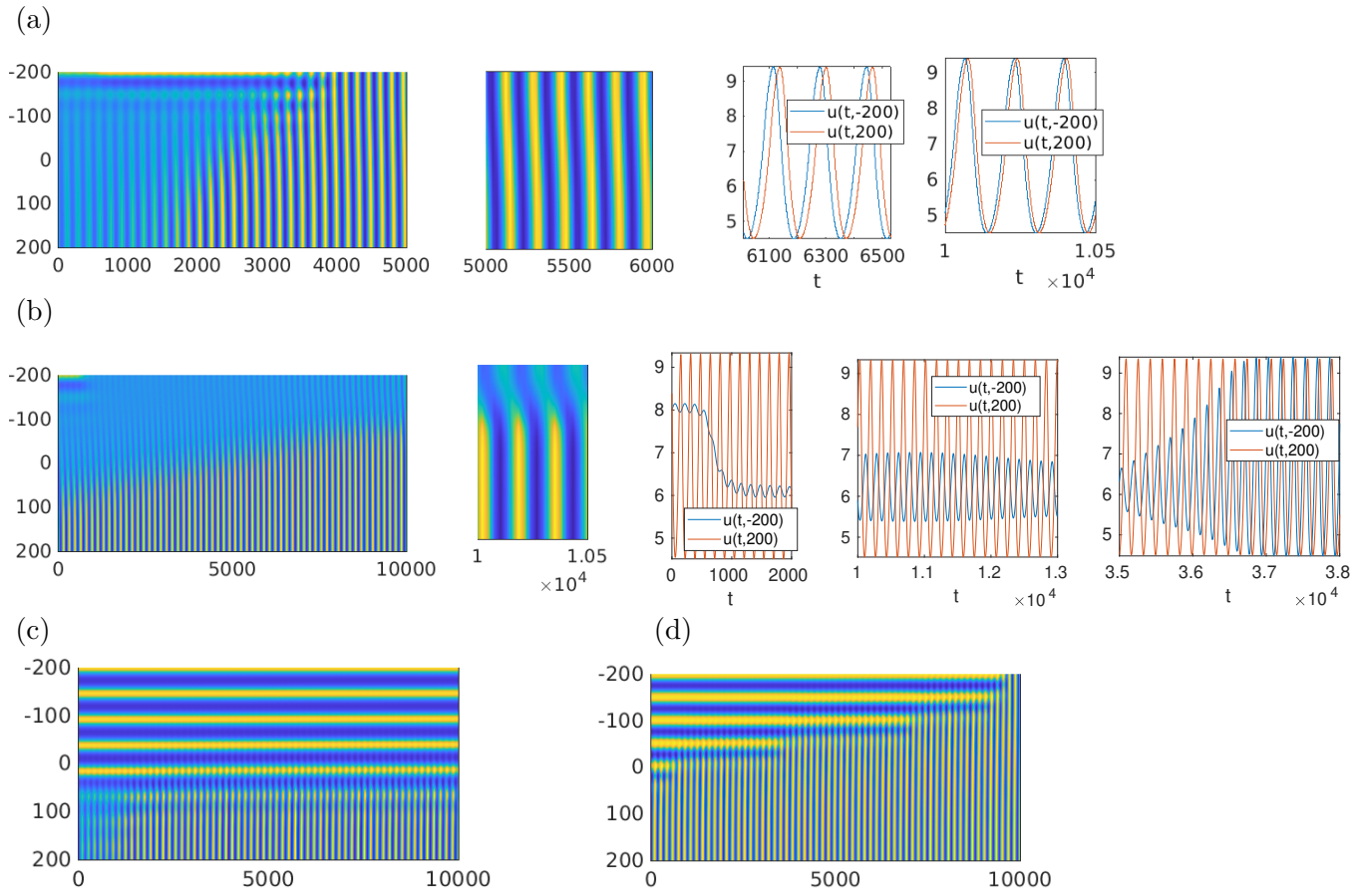

Figure 20: DNS starting from some states in Figs. 11 and 13. (a) Evolution from state A in Fig. 11, with late-time zoom and time-series at the left and right boundaries showing convergence towards H1, with very slow phase adjustment. (b) Evolution from state B in Fig. 13, likewise with very slow convergence to H1. (c) Evolution from state C in Fig. 13 with convergence to a THMM state. (d) Evolution from state E in Fig. 11 with convergence to H1 via stick-slip motion that gradually eliminates the Turing part of the IC.

Near $C2TH_1$ we identified bifurcations (HPs) on the LSS snake to both THMM states and to localized breathing states referred to as LSW, and employed numerical continuation to compute branches of both types as parameters varied. Both can come in stacks of short branch segments connecting different HPs on the classical LSS snake, or in long snaking branches that resemble classical LSS snakes. These possibilities can be connected using two-parameter continuation of the HPs and we have used this procedure to show how such stacks can zip up, i.e., recombine into snakes of time-periodic states, and how snakes can unzip, as parameters vary. Evidently, numerical continuation is an efficient procedure that can be used to uncover even quite complex (bifurcation) structures, provided the domain is not too large. However, on very large domains the profusion of (Hopf or steady) bifurcation points becomes overwhelming. In our case both THMM and LSW solutions are stable in some parameter regimes near $C2TH_1$, but significant parts of the parameter space seem to contain few stable solutions computable by our bifurcation approach up to tertiary bifurcations. We have therefore also used DNS to investigate the dynamics of (1), and found a further class of solutions combining LSW in one part of the domain with uniform Hopf oscillations in the remainder, see Figs. 6 and 8. These solutions are quasiperiodic in time rather than periodic and, moreover, the LSW part may oscillate irregularly or even chaotically in the sense of exhibiting frequent phase slips, as in Fig. 7. Such solutions are difficult if not impossible to compute using numerical continuation.

Near $C2TH_2$ we found no LSW branches, and the two-parameter continuation of the THMM branches is very different from that near $C2TH_1$. Starting with a value of the diffusion coefficient

D that yields stacks of (rather long) green connections of THMM type on the orange LSS snake in Fig. 13, changing D in either direction, we found no zipping up of THMM branches. Instead we were able to identify stacks of disconnected branches of THMM called isolas that arise because the HPs in which the THMM branches originate collide in a different way near the two codimension-2 points. This also explains *a posteriori* why in [Uec21a] we could not find large amplitude THMM by continuation and bifurcation alone because there we investigated the parameter regime with $(\alpha, D, \tau) = (0.02, 8, 0.05)$ where the large amplitude THMM are found only on isolas. Our present base choice $(\alpha, D, \tau) = (0.034, 6.5, 0.05)$ is much more suitable for uncovering the presence and formation of such solution isolas upon variation of D (and simultaneously works nicely near $\mathrm{C2TH}_1$ as well). We also explored the dynamics near $\mathrm{C2TH}_2$ via DNS, finding that here solutions converge to either Turing states or LSS, or to H1 or THMM, but often with very long transients (Fig. 20). Of course, as in all problems of this type, these approaches only generate a partial picture of the solution complexity.

The structures we have computed may be interpreted as possible defect structures in RD systems, with the Turing state representing the structure of the core region embedded in an oscillating background, cf. [DWLDB96, NRM17]. The Neumann BCs employed in this work allow solutions with a peak or a trough at the center of such states, here located at the left boundary, with fully localized solutions obtained via reflection in the boundary. Such solutions lie on distinct branches, and we have focused here on the case of a peak at the boundary resulting in localized Turing structures with an odd number of peaks. The use of Neumann BCs has another important consequence: It forces the time-dependent structures to remain stationary, i.e., it prevents a drift of the structure. As shown in [Rob24], when drift is permitted one can find an additional class of defect-type solutions that are asymmetric under spatial reflection. Our formulation of the problem eliminates the latter possibility.

A Movies

Some details of the branching structure are best understood from the movies associated to Fig. 2 (`mov1.avi`), Fig. 10 (`mov1b.avi`), and Fig. 11 (`mov2.avi`), available as supplementary material and also at [Uec24]. The general layout of the movies is explained in Fig. 21. When playing, a magenta marker moves through the BDs on the left, and the current solution and spectral information is shown on the right. Using a suitable player, we also recommend to go through these movies frame by frame.

References

[ACV24] F. Al Saadi, A. Champneys, and N. Verschueren. Snakes, ladders and breathers; organization of localized patterns in reaction-diffusion systems. *SIAM J. Appl. Dyn. Syst., submitted*, 2024.

[AGN24] F. Al Saadi, C. Gai, and M. Nelson. Localized pattern formation: semi-strong interaction asymptotic analysis for three components model. *Proc. R. Soc. A*, 480:20230591, 2024.

[AKNU24] F. Al Saadi, E. Knobloch, M. Nelson, and H. Uecker. Time-dependent localized patterns in a predator-prey model. *Chaos*, 34:043143, 2024.

[APR23] F. Al Saadi and P. Parra-Rivas. Transitions between dissipative localized structures in the simplified Gilad–Meron model for dryland plant ecology. *Chaos*, 33:033129, 2023.

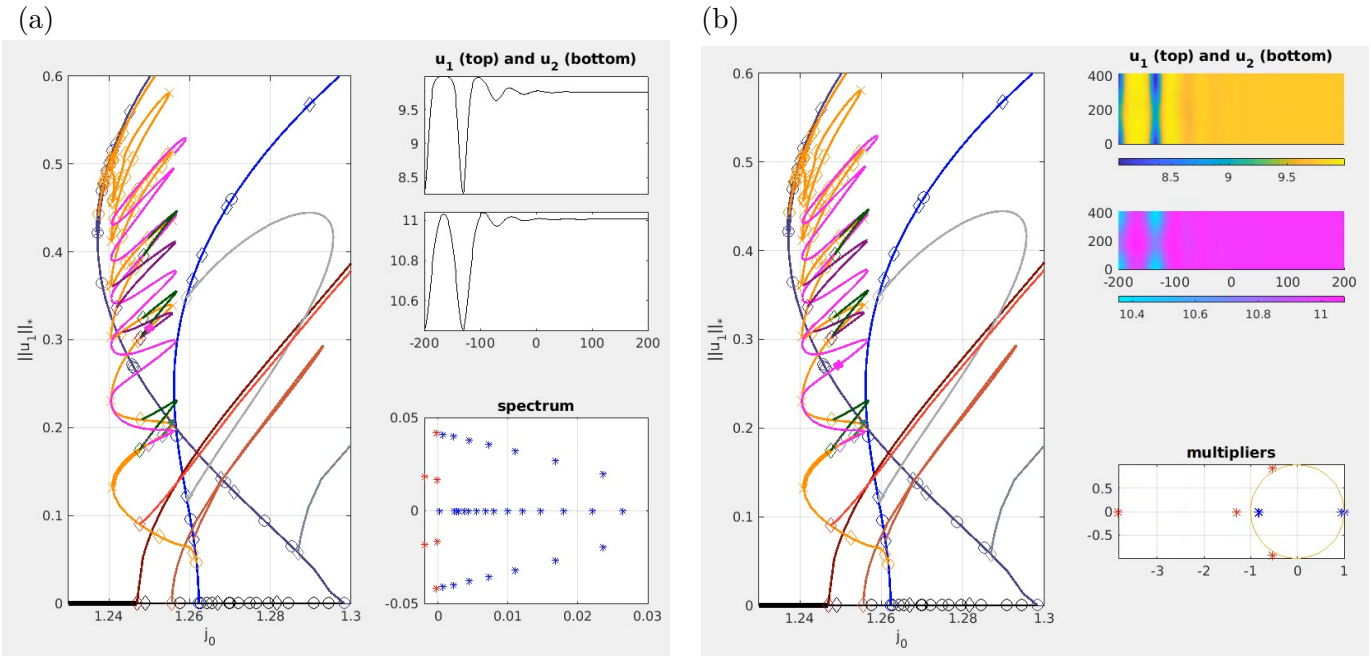

Figure 21: Snapshots from the movie `bdm1.avi`. Partial BD on the left, with a magenta marker for the current solution plotted on the right. (a) At a steady state we plot u_1 and u_2 (top right, x axis horizontal) and the spectrum (near 0) of the linearization around u (bottom right), with unstable eigenvalues μ (in `pde2path` meaning $\mathrm{Re}\mu < 0$) in red. (b) For a PO, we plot u_1 and u_2 over one period T (T along vertical axis, x axis horizontal) at the top right, while the bottom right shows the 20 largest Floquet multipliers, with those of modulus > 1 in red.

[AWAN22] F. Al Saadi, A. Worthy, H. Alrihieli, and M. Nelson. Localised spatial structures in the thomas model. *Mathematics and Computers in Simulation*, 194:141–158, 2022.

[BK07] J. Burke and E. Knobloch. Homoclinic snaking: Structure and stability. *Chaos*, 17:037102, 2007.

[BK09] J. Burke and E. Knobloch. Multipulse states in the Swift-Hohenberg equation. *Discrete and Continuous Dyn. Syst. Suppl.*, pages 109–117, 2009.

[BKL+09] M. Beck, J. Knobloch, D. J. B. Lloyd, B. Sandstede, and T. Wagenknecht. Snakes, ladders, and isolas of localized patterns. *SIAM J. Math. Anal.*, 41:936–972, 2009.

[CK09] S. J. Chapman and G. Kozyreff. Exponential asymptotics of localised patterns and snaking bifurcation diagrams. *Physica D*, 238:319–354, 2009.

[DWLDB96] A. De Wit, D. Lima, G Dewel, and P. Borckmans. Spatiotemporal dynamics near codimension-two point. *Phys. Rev. E*, 54:261–271, 1996.

[Kno08] E. Knobloch. Spatially localized structures in dissipative systems: open problems. *Nonlinearity*, 21:T45–T60, 2008.

[KUY21] E. Knobloch, H. Uecker, and A. Yochelis. Origin of jumping oscillons in an excitable reaction-diffusion system. *Phys. Rev. E*, 104:L062201, 2021.

[MDWBS97] M. Meixner, A. De Wit, S. Bose, and E. Schöll. Generic spatiotemporal dynamics near codimension-two Turing-Hopf bifurcations. *Phys. Rev. E*, 55:6690–6697, 1997.

[NRM17] Z. G. Nicolaou, H. Riecke, and A.E. Motter. Chimera states in continuous media: existence and distinctness. *Phys. Rev. Lett.*, 119:244101, 2017.

[Pom86] Y. Pomeau. Front motion, metastability and subcritical bifurcations in hydrodynamics. *Physica D*, 23:3–11, 1986.

[Rob24] T. V. Roberts. *Homoclinic Snaking of Spatiotemporal Patterns in Reaction Diffusion Systems*, PhD thesis, Brown University, RI, `https://repository.library.brown.edu/studio/item/bdr:y8vdpd2h/`, 2024.

[TBMV11] J. C. Tzou, A. Bayliss, B. J. Matkowsky, and V. A. Volpert. Interaction of Turing and Hopf modes in the superdiffusive Brusselator model near a codimension two bifurcation point. *Math. Model. Nat. Phenom.*, 6:87–118, 2011.

[TMB+13] J. C. Tzou, Y. P. Ma, A. Bayliss, B. J. Matkowsky, and V. A. Volpert. Homoclinic snaking near a codimension-two Turing–Hopf bifurcation bifurcation point in the Brusselator model. *Phys. Rev. E*, 87:022908, 2013.

[TMV09] J. C. Tzou, B. J. Matkowsky, and V. A. Volpert. Interaction of Turing and Hopf modes in the superdiffusive Brusselator model. *Appl. Math. Lett.*, 22:1432–1437, 2009.

[Uec21a] H. Uecker. Continuation and bifurcation for nonlinear PDEs – algorithms, applications, and experiments. *Jahresbericht DMV*, 2021.

[Uec21b] H. Uecker. *Numerical Continuation and Bifurcation in Nonlinear PDEs*. SIAM, Philadelphia, PA, 2021.

[Uec24] H. Uecker. `www.staff.uni-oldenburg.de/hannes.uecker/pde2path`, 2024.

[UW14] H. Uecker and D. Wetzel. Numerical results for snaking of patterns over patterns in some 2D Selkov-Schnakenberg reaction-diffusion systems. *SIAM J. Appl. Dyn. Syst.*, 13:94–128, 2014.

[vHPPRM04] J. von Hardenberg, A. Provencale, P. Parra-Rivas, and E. Meron. Ecosystem engineers: from pattern formation to habitat creation. *Phys. Rev. Lett.*, 93:098105, 2004.

[WC99] P. D. Woods and A. R. Champneys. Heteroclinic tangles and homoclinic snaking in the unfolding of a degenerate reversible Hamiltonian-Hopf bifurcation. *Physica D*, 129:147–170, 1999.

[Zho19] Jun Zhou. Bifurcation analysis of a diffusive predator-prey model with Bazykin functional response. *Int. J. Bifur. Chaos Appl. Sci. Engrg.*, 29:1950136, 2019.